vascular remodeling of resistance vessels remains to be clarified.

Adenoviral vectors can efficiently deliver genes to a wide variety of dividing and non-dividing cell types. However, one drawback with their use is that immunological elimination of infected cells often results in transient gene expression *in vivo*.[15] AAV vectors can efficiently transduce non-dividing skeletal muscle cells and achieve sustained expression of therapeutic genes with minimum inflammatory and immune responses.[16] The transduced muscle cells produce therapeutic proteins, which are secreted into the systemic circulation.

In this study, we hypothesized that an IL-10-mediated anti-inflammatory approach could also retard the progression of vascular remodeling in resistance artery. Here, we demonstrate that AAV-mediated sustained IL-10 expression prevents structural change in resistance artery and peripheral organ damage in the SHR-SP model.

Results

Expression of rat IL-10 in vitro *and* in vivo

To confirm the expression of AAV1RIL10 *in vitro*, total cell lysates of human embryonic kidney 293 (HEK293) cells transduced with recombinant AAV (rAAV), and the corresponding conditioned media, were prepared for western blot analysis of rat IL-10. IL-10 was detected in the conditioned medium of HEK293 cells transduced with AAV1RIL10, but not in the AAV1RIL10 cell lysate or the conditioned medium of HEK293 cells transduced with AAV1LacZ (Figure 1a). These results indicate that IL-10 is secreted from transduced cells. The biological activity of rat IL-10 was confirmed using lipopolysaccharide-stimulated rat splenocytes *in vitro*. After stimulation with lipopolysaccharide, splenocytes were incubated with the conditioned medium of HEK293 cells transduced with AAV1RIL10 or AAV1LacZ. Production of IFN-γ was suppressed by incubation with AAV1RIL10 but not with AAV1LacZ (data not shown), suggesting that rat IL-10 produced by AAV1RIL10 was biologically active. The serum IL-10 concentration in the SHR-SP transduced with rAAV vectors is shown in Figure 1b. Three weeks after gene delivery, serum IL-10 was elevated in a dose-dependent manner and this remained stable over a 6-month period.

Stroke-free duration and neurological score of SHR-SP

To analyze whether stable expression of IL-10 can modify the frequency of stroke episodes in the SHR-SP, the incidences of stroke-associated symptoms were observed (Figure 2a). Although all control rats (injected with AAV1LacZ or saline) showed stroke-associated symptoms, no stroke-associated symptoms were observed in the rats transduced with AAV1RIL10 (1×10^{11} or 1×10^{12} genome copies per body (g.c. per body)), even more than 7 months after gene delivery. As the SHR-SP stroke episodes are usually temporary and associated neurological deficits fluctuate significantly at an early stage, the SHR-SP neurological score was determined 6 months after gene delivery. As shown in Figure 2b, control rats revealed marked deterioration, whereas rats transduced

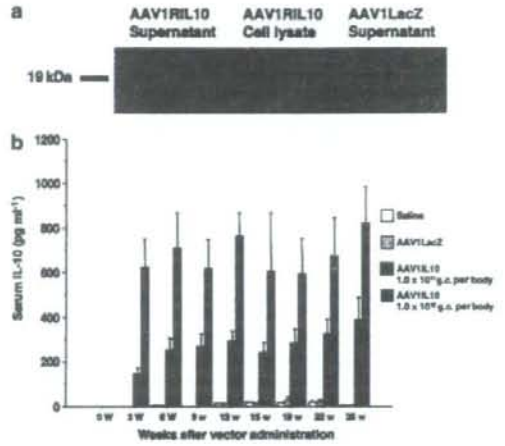

Figure 1 Long-term rAAV-mediated expression of rat IL-10 *in vivo*. (**a**) Expression of rat IL-10 in HEK293 cells. Total cell lysates of HEK293 cells were transduced with rAAVs, and the corresponding conditioned medium was probed with an antibody against rat IL-10. Rat IL-10 was detectable in conditioned medium (lane 1) of HEK293 cells transduced with AAV1RIL10 at 1×10^4 g.c. per cell but not in the corresponding cell lysate (lane 2). It was also undetectable in conditioned medium of HEK293 cells transduced with AAV1-LacZ (lane 3). (**b**) Serum IL-10 concentration in the SHR-SP. AAV1RIL10 (1×10^{11} or 1×10^{12} g.c. per body), AAV1LacZ (1×10^{11} g.c. per body) or saline was injected into the bilateral anterior tibial muscles of the male SHR-SP at 6 weeks of age. Serum concentration of rat IL-10 was measured periodically by ELISA after gene delivery. Values represent mean ± s.d. ($n = 5$ for each group). ELISA, enzyme-linked immunosorbent assay; g.c., genome copies; IL, interleukin; rAAV, recombinant AAV; SHR-SP, stroke-prone spontaneously hypertensive rat.

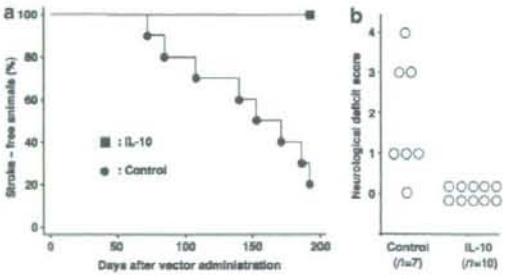

Figure 2 Prevention of stroke episodes in the IL-10-transduced SHR-SP. (**a**) Stroke-free duration of SHR-SP. Male SHR-SP were injected with AAV1RIL10 (IL-10, 1×10^{11} or 1×10^{12} g.c. per body, $n = 5$ each), AAV1LacZ (1×10^{11} g.c. per body, $n = 5$) or saline ($n = 5$) in the bilateral anterior tibial muscles at 6 weeks of age. Control group is comprised of the AAV1LacZ-injected animals and saline-injected animals. Seizure, paralysis of hindlimb, as well as decreased activity, were all regarded as symptoms. Rats were behaviorally assessed every day. The percentage of stroke-free animals was analyzed by the Kaplan–Meier method. The AAV1-RIL10-treated group showed significantly prolonged stroke-free duration compared with the control group ($P < 0.001$). (b) Neurological deficit scores of SHR-SP. Six months after gene delivery, neurological deficits were evaluated according to a scoring system described in the Materials and methods section. $P < 0.005$ vs control group. g.c., genome copies; IL, interleukin; SHR-SP, stroke-prone spontaneously hypertensive rat.

with the AAV1RIL10 (1×10^{11} or 1×10^{12} g.c. per body) showed no neurological deficits at this time point.

Histological evaluation and immunohistochemical examination of the cerebral parenchyma

Representative morphological changes and immunohistochemical analysis in the cerebral parenchyma are shown in Figure 3. Multiple ischemic foci (Figure 3a) and hyalinotic changes of the arterioles with perivascular cystic change (Figure 3c) were observed in the vehicle-treated group 7 months after gene delivery. In the AAV1RIL10-treated group, arteriolosclerosis and ischemic foci were negligible across the whole brain at the same time point (Figures 3b and d). Seven months after gene delivery, marked infiltration of ED1-positive (Figure 3e) or CD11b-positive cells (Figure 3g) was observed around the pial arterioles of the cerebral parenchyma in the vehicle-treated group. In the AAV1-RIL10-treated group, infiltration of ED1-positive (Figure 3f) or CD11b-positive cells (Figure 3h) in the pial arterioles was rare. Immunoreactivity of collagen type IV on the vessel walls was also higher in the control brain than in the AAV1RIL10-treated brain (Figures 3i and j).

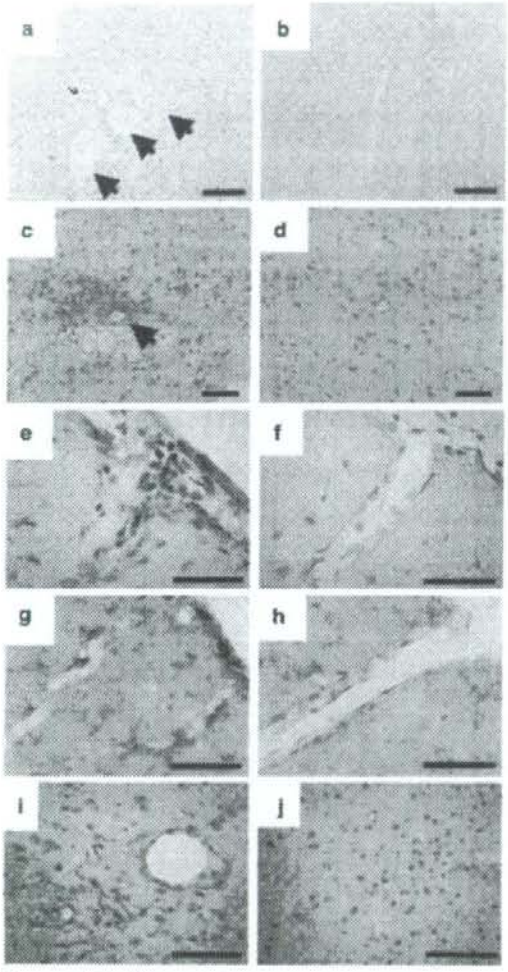

Figure 3 Morphological changes and immunohistochemical examination in the cerebral parenchyma. SHR-SP was transduced with AAV1LacZ (**a**, **c**, **e**, **g** and **i**) or AAV1RIL10 (**b**, **d**, **f**, **h** and **j**). Morphological changes were evaluated by hematoxylin and eosin (HE; **a** and **b**) and periodic acid Schiff stain (PAS; **c** and **d**) at 7 months after gene delivery. Scale bars: 100 μm (**a** and **c**) and 50 μm (**b** and **d**). Representative immunohistochemical examination of the brain at 7 months after gene delivery (**e**–**j**). Immunohistochemical analysis of cells expressing ED1 (**e** and **f**) or CD11b (**g** and **h**) or collagen type IV (**i** and **j**) in the cerebral parenchyma of the transduced animals. Scale bars: 100 μm (**e**–**j**). SHR-SP, stroke-prone spontaneously hypertensive rat.

Protected renal function in SHR-SP

To assess the progression of renal damage, urine was collected over a 24-hour period from rats housed in metabolic cages at 8, 12, 16 and 24 weeks after gene delivery and proteinuria was evaluated. Although the vehicle-treated group showed a significant increase in proteinuria with age, in the AAV1RIL10-transduced group, proteinuria remained low (Figures 4a). Representative morphological changes in the kidney at 7 months after gene delivery are shown in Figures 4b–e. The vehicle-treated group had major cortical damage including decreased cell height, loss of brush borders in the proximal tubules, sclerotic glomeruli, accumulated colloid or protein casts and focal accumulation of inflammatory cells (Figure 4b). Arteriolar fibrinoid necrosis was also apparent in the vehicle-treated group (Figure 4c). However, in the AAV1RIL10-transduced group, normal kidney structure was preserved (Figure 4d) and arteriolar fibrinoid necrosis was rarely seen (Figure 4e) at 7 months after gene delivery.

Immunohistochemical examination of the kidney

Representative immunohistochemical examination of the kidney at 7 months after gene delivery is shown in Figure 5. Marked infiltration of ED1-positive cells was observed in the small arteries of the control group (Figure 5a) compared with the AAV1RIL10-treated group (Figure 5b). Intense transforming growth factor (TGF)-β immunoreactivity in proximal tubular epithelial cells was also evident in the vehicle-treated group (Figure 5c) compared with the AAV1RIL10-treated group (Figure 5d). Infiltration of nuclear factor (NF)-κB p65 subunit-positive cells was also detected in the small arteries (Figures 5e and f) and proximal tubules (Figures 5g and h) in the control group. In contrast, infiltration of NF-κB p65 subunit-positive cells in either the vessel wall (Figure 5i) or interstitium (Figure 5j) was barely detectable in the AAV1RIL10-treated group.

Serum biochemistry

Aspartate aminotransferase (AST), alanine aminotransferase (ALT), total cholesterol, blood urea nitrogen and creatinine significantly decreased in the AAV1RIL10-treated group at 6 months after transduction (Table 1). Serum albumin, glucose and triglyceride were significantly decreased in the control group. Serum cytokine concentration profile is also summarized in Table 1. IFN-γ and TGF-β concentrations significantly decreased in the AAV1RIL10-treated group at 6 weeks after transduction.

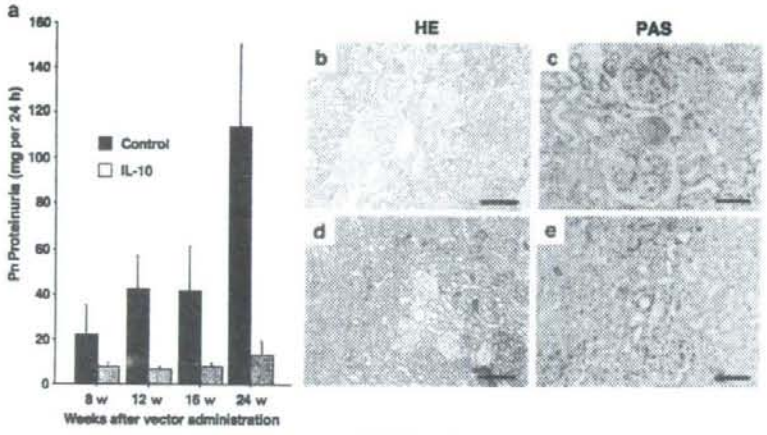

Figure 4 Prevention of renal dysfunction in the IL-10-transduced SHR-SP. (a) Reduction of proteinuria in SHR-SP. The transduction protocol is identical to that used in Figure 2. Urine was collected from rats in metabolic cages for a 24-hour period at 8, 12, 16 and 24 weeks after gene delivery and then proteinuria was evaluated. SHR-SP transduced with AAV1RIL10 showed a significant reduction in proteinuria ($P<0.001$, $n=10$ for each group). Data are shown as mean ± s.d. Representative morphological changes in the kidney of SHR-SP transduced with AAV1LacZ (b and c) or AAV1RIL10 (d and e) were evaluated by hematoxylin and eosin (HE; b and d) and periodic acid Schiff stain (PAS; c and e) at 7 months after gene delivery. Scale bars: 100 μm (b and d) and 50 μm (c and e). IL, interleukin; SHR-SP, stroke-prone spontaneously hypertensive rat.

Blood pressure of SHR-SP and morphological changes in the carotid artery

Systolic blood pressure of the SHR-SP is shown in Figure 6. At 6 weeks of age, systolic blood pressure in the control and AAV1RIL10-treated groups was equivalent. Blood pressure gradually increased with age in the control group and reached a plateau of approximately 210–230 mm Hg at 16 weeks of age. Interestingly, systolic blood pressure in the AAV1RIL10-transduced group plateaued at lower values than controls. This effect on the systolic blood pressure persisted over 30 weeks after transduction (Figure 6a). A significant correlation was observed between serum IL-10 concentration and systolic blood pressure at 9 weeks after transduction (Figure 6b). Histological changes in the carotid artery 6 months after vector administration are summarized in Figure 6c. Compared with the control group, carotid artery integrity was well preserved in the AAV1RIL10-treated group. Quantitative analysis of carotid diameter and media thickness is shown in Figure 6d. Both of these parameters decreased significantly in the AAV1RIL10-treated group.

Prolonged survival of SHR-SP

Survival of SHR-SP transduced with AAV1RIL10 (1×10^{11} or 1×10^{12} g.c. per body), AAV1LacZ or saline was evaluated by Kaplan–Meier survival analysis (Figure 7). Transduction of the SHR-SP with AAV1RIL10 significantly prolonged survival compared with that of controls (AAV1LacZ or saline; $n=10$ for each group; $P<0.001$).

Discussion

Here we demonstrate that sustained IL-10 expression can prevent the progression of arteriolosclerosis and associated target-organ damage in the SHR-SP. A single intramuscular injection of an AAV1-based vector encoding IL-10 achieved long-term systemic IL-10 expression. The resultant IL-10-transduced rats showed an improvement in proteinuria, as well as prolonged stroke-free duration and survival. Histological examination revealed a reduction in brain arteriolosclerosis and nephrosclerosis when compared with control rats. Immunohistochemical examination confirmed decreased infiltration of monocytes/macrophages and NF-κB-positive cells in the brain and renal arteriolosclerotic lesions of these rats. IL-10-transduced rats also exhibited a sustained decrease in the systolic blood pressure compared with controls.

The AAV vector, derived from a non-pathogenic parvovirus, can transduce non-dividing neuronal and skeletal muscle cells, and can also achieve long-term transgene expression *in vivo* with minimal inflammatory and immune responses.[17,18] Intramuscular injection of the vector is used to transduce the skeletal muscle *in vivo* and the resultant transduced muscle cells produce the encoded proteins, which are secreted into the systemic circulation. Preclinical and clinical investigations using AAV2-based vectors have demonstrated efficient neuronal transduction and therapeutic benefits in neurodegenerative diseases with minimum adverse effects.[18] However, the application of this technique might be limited because of insufficient levels of transgene expression in other tissues.[19] The AAV serotype 1-based vector has distinct receptors that may promote the initial viral binding and entry into muscle cells, leading to a more efficient transduction to skeletal muscle than AAV2-based vectors.[20] We therefore utilized an AAV1-pseudotyped vector in this study. We confirmed the presence of sustained and adequate IL-10 serum levels in SHR-SP after a single intramuscular injection of AAV1IL10.

We initially evaluated the effects of IL-10 on SHR-SP behavior. IL-10-tranduced rats showed decreased stroke-associated symptoms compared with the untreated controls. This behavioral improvement might be

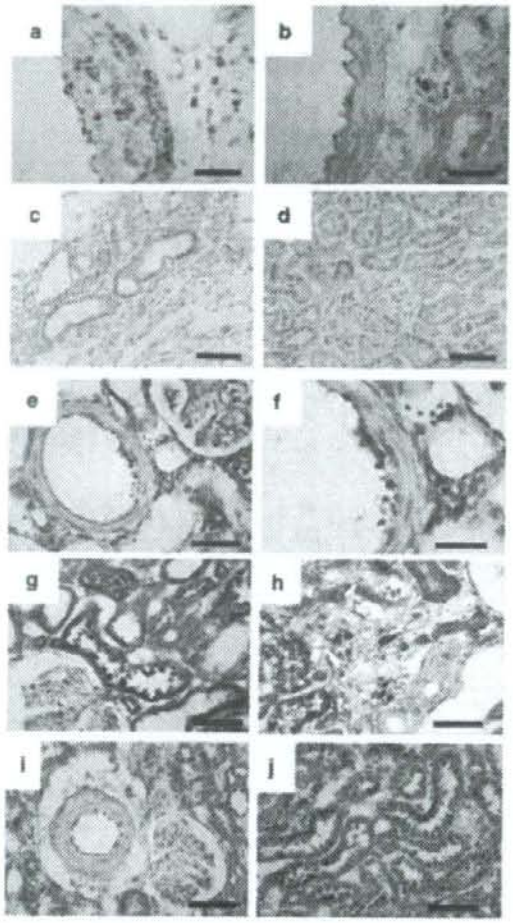

Figure 5 Immunohistochemical examination of the kidney at 7 months after gene delivery. Immunohistochemical detection of cells expressing ED1 (**a** and **b**) or TGF-β (**c** and **d**) or NF-κB p65 subunit (**e**–**j**) in the kidney of the SHR-SP transduced with AAV1LacZ (**a**, **c**, **e**, **f**, **g** and **h**) or AAV1RIL10 (**b**, **d**, **i** and **j**). Scale bars: 30 μm (**a**, **b** and **f**) and 50 μm (**c**–**e** and **g**–**j**). NF-κB, nuclear factor-κB; SHR-SP, stroke-prone spontaneously hypertensive rat; TGF-β, transforming growth factor-β.

Table 1 Serum biochemical analysis of AAV-transduced SHR-SP

	Control (n = 9)	*IL-10* (n = 10)
AST	57.8 ± 13.1	35.5 ± 6.2***
ALT	89.5 ± 8.0	59.0 ± 17.0**
Albumin	3.9 ± 0.2	4.7 ± 0.1***
Total cholesterol	107.1 ± 22.5	64.2 ± 3.2***
Triglyceride	57.3 ± 39.4	69.3 ± 12.6*
Glucose (fasting)	117.6 ± 9.7	145.1 ± 13.2***
Blood urea nitrogen	28.8 ± 7.0	17.8 ± 2.1**
Creatinine	0.37 ± 0.06	0.22 ± 0.01***
	Control (n = 10)	*IL-10* (n = 10)
IFN-γ	2.88 ± 1.02	1.59 ± 0.45††
TGF-β	18.0 ± 2.6	15.1 ± 2.6†

Abbreviations: AAV, adeno-associated virus; SHR-SP, stroke-prone spontaneously hypertensive rat.
The transduction protocol is identical to that used in Figure 2. Serum biochemical analysis of the SHR-SP was performed at 6 months after injection. Serum cytokine profile in the AAV1RIL10-transduced SHR-SP (IL-10) or saline-treated SHR-SP (control) was also analyzed at 6 weeks after injection. Each value is the mean ± s.d.
*$P < 0.01$, **$P < 0.005$, ***$P < 0.001$, versus control SHR-SP.
†$P < 0.05$, ††$P < 0.005$, versus control SHR-SP.

explained by IL-10-mediated vasculoprotection, although demonstrating direct neuroprotective effects of IL-10 would require further experimentation. Our results indicate that the vasculoprotective effects of IL-10 might be associated with its anti-inflammatory properties. Accumulating evidence supports the notion that hypertension is the biggest risk factor for brain lacunar syndrome and intracerebral hemorrhage, suggesting that high blood pressure affects the local injury of intracerebral arteries.[21] Degenerative vascular changes, similar to those seen in human essential hypertensives, occur in the brain of the SHR and SHR-SP.[22] We demonstrated that long-term systemic IL-10 expression prevented the arteriolosclerotic lesions, normally characterized by fibrinoid necrosis and monocyte/macrophage infiltration, in cerebral arteries of the SHR-SP. We also observed reduced serum levels of IFN-γ, a proinflammatory cytokine released by Th1 cells, in the IL-10-transduced rats. A Th1-dominant T-cell population is associated with progression of hypertensive organ damage.[17] However, IL-10 is reported to deactivate monocytes by reducing IFN-γ production,[23] thereby improving atherosclerotic lesions by shifting the Th pattern from Th1-dominant to Th2-dominant. These observations suggest that IL-10 might regulate vascular inflammation by modulating Th imbalance. In addition, IL-10 inhibits the expression of adhesion molecules and matrix metalloproteinases, as well as smooth muscle cell proliferation.[24–28] These IL-10 effects might regulate local vascular inflammation and remodeling, also leading to an improvement in arteriolosclerosis. Clearly, further investigations are required to clarify the mechanism(s) by which IL-10 improves hypertension-associated vascular damage in more detail.

In this study, we also observed that activated NF-κB-positive cells accumulate in renal arteriolosclerotic lesions of the SHR-SP. The transcription factor, NF-κB, is activated by a wide variety of proinflammatory molecules, such as IL-8, macrophage chemotactic protein-1, intercellular adhesion molecule-1, vascular-cell adhesion molecule-1 and E-selectin.[29–31] Monocyte infiltration into the small renal arteries stimulates NF-κB activation, leading to chemokine and cytokine expression in the kidney. NF-κB is also known to be activated in the course of vascular inflammation and renal injury in the SHR.[32] In contrast, IL-10 directly inhibits NF-κB activation in macrophages.[33] In this study, IL-10-transduced rats showed a decrease in activated NF-κB-positive cells in the renal arteriolosclerotic lesions of SHR-SP, which might reflect reduced inflammatory activity within these lesions.

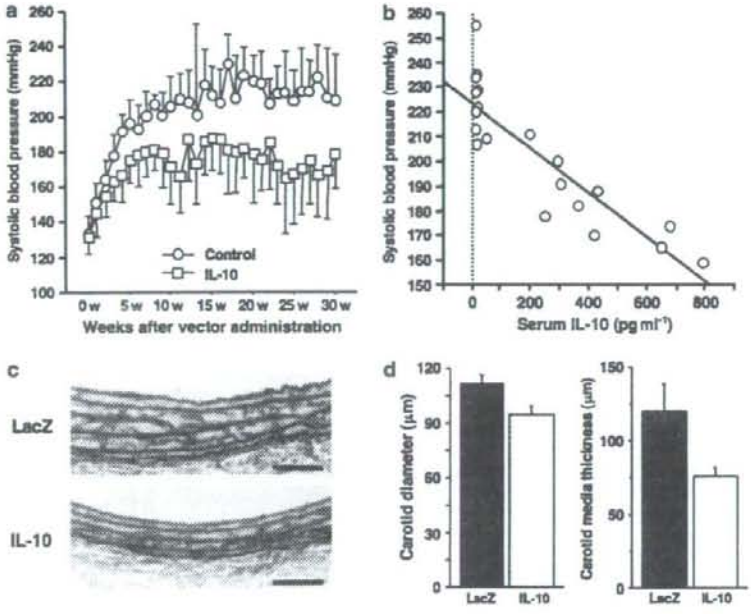

Figure 6 Decrement of blood pressure and morphological changes of carotid artery in the IL-10-transduced SHR-SP. (**a**) Systolic blood pressure of SHR-SP. The transduction protocol is identical to that used in Figure 2. Systolic blood pressure was evaluated by the tail-cuff method. Data are shown as mean ± s.d. (**b**) Correlation between serum IL-10 concentration and blood pressure at 9 weeks after transduction ($n = 20$; $r = 0.882$; $P < 0.0001$). (**c**) Morphological change of the carotid artery after vector administration. Histological changes in the carotid artery of LacZ-transduced group and IL-10-transduced group were evaluated by elastica van Gieson staining at 6 months after gene delivery. Scale bars: 100 μm. (**d**) Quantitative analysis of carotid diameter and media thickness at 6 months after gene delivery. Both the carotid diameter and media thickness were significantly decreased in the IL-10-transduced group than in the LacZ-transduced group ($n = 5$ for each group, $^*P < 0.01$). IL, interleukin; SHR-SP, stroke-prone spontaneously hypertensive rat.

We further investigated the role of TGF-β in renal arteriolosclerosis and nephrosclerosis. TGF-β, a multifunctional growth factor, plays an important role in tissue repair and fibrosis by regulating cell proliferation and differentiation. Recent evidence supports the notion that overproduction of TGF-β may cause the vascular remodeling and other long-term sequelae of hypertension, including nephrosclerosis.[34,35] TGF-β may regulate blood pressure levels by stimulating endothelin-1 mRNA expression and releasing renin from the juxtaglomerular cells of the kidney.[34,36] It can also increase vascular compliance by promoting deposition of extracellular matrix components in the vessel walls.[37] Moreover, treatment of the Dahl salt-sensitive rat strain with an anti-TGF-β antibody significantly reduces blood pressure, proteinuria and albuminuria.[38] In the SHR-SP, glomerular and tubulointerstitial TGF-β expression, as well as cellular phenotypic modulation, accelerates the progression of renal fibrosis and nephrosclerosis.[39] Enhanced TGF-β expression also promotes the hypoxia-induced tubulointerstitial transdifferentiation of proximal tubular cells.[40] We found evidence for renal arteriolosclerosis and nephrosclerosis, along with enhanced TGF-β expression, in the renal epithelial cells and sera of the SHR-SP. In contrast, the IL-10-transduced rats had preserved renal structures and decreased TGF-β expression compared with the controls. These results indicate that IL-10-mediated TGF-β regulation may be involved in the physiological protective mechanism against renal arteriolosclerosis and the emergence of hypertension.

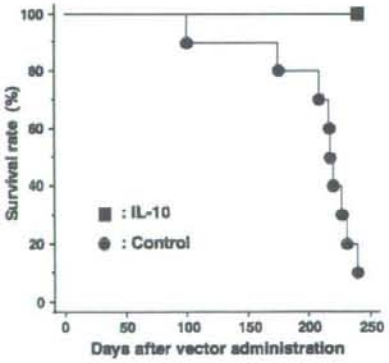

Figure 7 Improved survival of the IL-10-transduced SHR-SP. Survival after transduction of the SHR-SP was estimated by Kaplan–Meier analysis. The experimental protocol is identical to that used in Figure 2. The SHR-SP transduced with AAVRIL10 showed significantly prolonged survival ($P < 0.001$). IL, interleukin; SHR-SP, stroke-prone spontaneously hypertensive rat.

The cholesterol-lowering effect of sustained, systemic IL-10 expression we observed is consistent with our earlier study.[7] The decreased levels of glucose and triglyceride that appeared in the control group may be associated with malnutrition after stroke episodes. Decreased serum albumin levels in this group might result from proteinuria caused by hypertensive renal dysfunction. Importantly, serological studies showed no apparent adverse effects in the IL-10-transduced group.

As a first step toward the future therapeutic investigation, we tried rAAV-mediated IL-10 transduction to prevent vascular remodeling and inflammatory lesions in this study. Here, we have shown protective function of IL-10 against malignant hypertension, although it would be more important to investigate the therapeutic effect on developed hypertension. This protective approach also provides significant insights into the prevention strategy of disease onset in patients with genetic predisposition or intractable polygenic disorders.

In conclusion, we have provided the first evidence that AAV vector-mediated stable IL-10 expression prevents arteriolosclerosis and end-organ damage in the SHR-SP, leading to decreased stroke episodes and prolonged survival. Although the mechanisms underlying the antihypertensive effect of IL-10 require further clarification, its vasculoprotective effect might involve an anti-inflammatory process. Our results suggest that IL-10-mediated vascular protection would be an alternative effective therapeutic strategy to prevent the progression of refractory hypertensive disorders.

Materials and methods

Cloning of rat IL-10 and plasmid construction

Rat IL-10 was cloned from cDNA of rat splenocytes by PCR using the following primers: 5′-GCACGAGAGC CACAACGCA and 5′-GATTTGAGTACGATCCATT TATTCAAAACGAGGAT. The 1.3-kb PCR product was cloned into pCR2.1 by using a TA cloning kit (Invitrogen Corp., Carlsbad, CA, USA). The cloned PCR-amplified fragment was verified by sequencing. The resultant plasmid, pCR2.1RatIL-10, was digested with *Eco*RI, and then the rat IL-10 gene fragment was inserted into the *Eco*RI site of p3.3CAG-WPRE, which contains a CAG promoter and woodchuck post-transcriptional regulatory element (WPRE). Finally, the entire expression cassette was inserted between the AAV2-derived inverted terminal repeats (ITRs) in a pUC-based proviral plasmid, pAAVLac Z, to form pWCAGRIL10W.

Recombinant adeno-associated virus production

Recombinant AAV was propagated according to a three-plasmid transfection adenovirus-free protocol.[41] Briefly, 60% confluent HEK293 cells were co-transfected with the proviral plasmid (pWCAGRIL10W or pAAVLac Z), AAV-1, chimeric helper plasmid, p1RepCap, and adenoviral helper plasmid, pAdeno, to produce rAAV expressing either rat IL-10 (AAV1RIL10) or *Escherichia coli* β-galactosidase gene (AAV1LacZ). Resultant crude virus lysates were purified through two rounds of CsCl two-tier centrifugation.[16] The physical titer of the viral stock was determined by dot blot hybridization with plasmid standards.

Western blot analysis and functional analysis of rat IL-10 in vitro

HEK293 cells were infected with AAV1RIL10 or AAV1-LacZ at 1×10^4 g.c. per cell. The supernatant and cell lysate were harvested 72 h after infection. Cells were lysed in a lysis buffer (10 mM Tris-HCl, 150 mM NaCl and 1% NP-40 (pH 7.6)) with Complete Mini (Roche Diagnostics, Mannheim, Germany). The supernatant was concentrated 10-fold using centricon YM-10 (Millipore, Bedford, MA, USA). Ten micrograms of cell lysate or 10 μl of concentrated conditioned medium was subjected to electrophoresis on 10% SDS-polyacrylamide gel electrophoresis under reducing conditions and transferred to a nitrocellulose membrane. The membrane was blocked and incubated with a 1:1000 dilution of mouse anti-rat IL-10 polyclonal antibody (Genzyme Techne, Minneapolis, MN, USA). The membrane was then rinsed and incubated with a 1:1000 dilution of peroxidase-linked anti-mouse IgG antibody (Amersham Pharmacia Biotech, Buckinghamshire, UK). Immunoreactive bands were visualized using the ECL Western blotting kit (Amersham). The biological activity of rat IL-10 was determined as follows: HEK293 cells were transduced with AAV1RIL10 at 1×10^4 g.c. per cell. Seventy-two hours after infection, this supernatant was recovered and the concentration of IL-10 in the supernatant was determined using the Rat Biotrak ELISA System (Amersham). Rat primary splenocytes were incubated with the IL-10-containing supernatant. Thirty minutes after incubation, lipopolysaccharides were added at a concentration of 10 ng ml^{-1}. Twenty-four hours later, the concentration of IFN-γ in the supernatant was determined using the Rat Biotrak ELISA System (Amersham).

Intramuscular injection of rAAV and physiological analysis

Male SHR-SP at 6 weeks of age were purchased from Japan SLC (Shizuoka, Japan) and used in the transduction study. The rats were housed under controlled conditions of constant temperature and humidity and exposed to 12-h light/dark cycle. The rats had free access to chow and tap water. All animal studies were performed in accordance with the guidelines issued by the committee on animal research of Jichi Medical School and approved by its ethics committee.

Male SHR-SP were injected with AAV1RIL10 (1×10^{11} or 1×10^{12} g.c. per body; $n = 5$ for each group), AAV1-LacZ (1×10^{11} g.c. per body; $n = 5$) or saline ($n = 5$) into the bilateral anterior tibial muscles at 6 weeks of age. Control group comprised AAV1LacZ-injected animals and saline-injected animals. From 8 weeks of age, rats were fed a controlled diet (Funahashi SP diet; Funahashi, Chiba, Japan). The systolic blood pressure of rats was measured weekly using a manometer tachometer (Natsume KN-210; Natsume Seisakusho, Tokyo, Japan) with a tail-cuff method. An average of five readings was recorded for each animal after they had acclimatized to the environment. Urine was collected from rats in metabolic cages for a 24-h period at 8, 12, 16 and 24 weeks after gene delivery. Urinary protein levels were determined by the Lowry method. Rats were monitored on a daily basis for behavioral signs of stroke. Stroke-associated symptoms, such as seizure, hindlimb

paralysis and decreased activity, were also assessed as physiological parameters. When any one of these symptoms occurred in the SHR-SP, animals were regarded as stroke positive. Six months after gene delivery, neurological deficits were evaluated according to the following scoring system:[42] (0) normal; (1) slight decrease in motor activity; (2) marked decrease in motor activity or hyperirritability; (3) no walking (decreased responsiveness); (4) inability to stand without support or paralysis of hindlimbs.

Serum biochemistry

Serum samples were collected from the tail vein and stored at −80 °C. Serum biochemistry values, including the concentration of albumin, AST, ALT, total cholesterol, triglyceride, glucose, blood urea nitrogen and creatinine, were estimated using standard procedures. IFN-γ, IL-4 and IL-10 concentrations in sera were measured by using a BIOTRAK ELISA system (Amersham). The concentration of TGF-β was determined by commercial enzyme-linked immunosorbent assay (BioSource International, Camarillo, CA, USA).

Histological examination

Seven months after gene delivery, anesthetized rats were perfused with 50 ml of saline, followed by 100 ml of cold 4% paraformaldehyde in 0.1 M phosphate buffer (pH 7.4). The brain, kidney, descending aorta and carotid artery were fixed in the same fixative and finally embedded in paraffin. Three-micrometer thick sections were stained with hematoxylin and eosin, periodic acid Schiff, oil red O and elastica van Gieson by standard methods for light microscopy.

Immunohistochemistry

Immunohistochemical staining was performed using a standardized streptavidin-bioin-peroxidase method. A mouse monoclonal antibody against rat ED1 (1:100; Serotec, Oxford, UK), a mouse monoclonal antibody against rat CD11b (1:100; Serotec), a rabbit polyclonal antibody against human collagen type IV (1:100; Progen, Heidelberg, Germany), a mouse monoclonal antibody against TGF-β (1:100; Chemicon, Temecula, CA, USA) and a mouse monoclonal antibody against NF-κB p65 subunit (1:50; Chemicon) were used as primary antibodies. Seven months after gene delivery, anesthetized rats were perfused, as described above. Four hours after fixation, the brain and kidney were transferred to 30% sucrose in 0.1 M phosphate buffer (pH 7.4) for cryoprotection and stored at 4 °C overnight. The tissue was frozen in OCT compound (Tissu-Tek; Sakura Finetek, Torrance, CA, USA) at −20 °C and 10-μm thick sections were sliced with a cryostat. The sections were washed and permeabilized with phosphate-buffered saline (PBS) containing 0.5% Triton-X for 10 min, followed by incubation in PBS containing 50 mM glycine. Slides were then washed three times with PBS and blocked with PBS containing 1% bovine serum albumin for 20 min. Internal peroxidase activity was quenched by incubation in PBS buffer containing 0.3% hydrogen peroxide with 0.1% sodium azide. After washing with PBS for three times, the sections were incubated with primary antibodies overnight at 4 °C followed by incubation with biotinylated anti-rabbit or anti-mouse IgG antibody (Vector Laboratories, Burlingame, CA, USA) and horse radish peroxidase-labeled streptavidin (Vector Laboratories). The reaction was visualized by using the Vector SG kit (Vector Laboratories), and nuclear fast red was used for counterstaining.

Acknowledgements

We thank Dr James M Wilson for providing p1RepCap (identical to p5E18RXCI). We thank Avigen Inc. (Alamada, CA, USA) for providing pAAVLacZ and pAdeno. We thank Dr Thomas Hope for providing WPRE DNA. We also thank Ms Miyoko Mitsu and Ms Naomi Inaba for their encouragement and technical support. This work was supported in part by grants from the Ministry of Health, Labour and Welfare of Japan: grants-in-aid for Scientific Research; grant for twenty-first century COE program; and 'High-Tech Research Center' Project for Private Universities, matching fund subsidy, from the Ministry of Education, Culture, Sports, Science and Technology of Japan.

References

1 Elenkov IJ, Chrousos GP. Stress hormones, proinflammatory and antiinflammatory cytokines, and autoimmunity. *Ann N Y Acad Sci* 2002; **966**: 290–303.
2 Fearon DT, Locksley RM. The instructive role of innate immunity in the acquired immune response. *Science* 1996; **272**: 50–53.
3 Ross R. Atherosclerosis—an inflammatory disease. *N Engl J Med* 1999; **340**: 115–126.
4 Mallat Z, Besnard S, Duriez M, Deleuze V, Emmanuel F, Bureau MF *et al*. Protective role of interleukin-10 in atherosclerosis. *Circ Res* 1999; **85**: e17–e24.
5 Pinderski LJ, Fischbein MP, Subbanagounder G, Fishbein MC, Kubo N, Cheroutre H *et al*. Overexpression of interleukin-10 by activated T lymphocytes inhibits atherosclerosis in LDL receptor-deficient mice by altering lymphocyte and macrophage phenotypes. *Circ Res* 2002; **90**: 1064–1071.
6 Von Der Thusen JH, Kuiper J, Fekkes ML, De Vos P, Van Berkel TJ, Biessen EA. Attenuation of atherogenesis by systemic and local adenovirus-mediated gene transfer of interleukin-10 in LDLr−/− mice. *FASEB J* 2001; **15**: 2730–2732.
7 Yoshioka T, Okada T, Maeda Y, Ikeda U, Shimpo M, Nomoto T *et al*. Adeno-associated virus vector-mediated interleukin-10 gene transfer inhibits atherosclerosis in apolipoprotein E-deficient mice. *Gene Therapy* 2004; **11**: 1772–1779.
8 Luft FC, Mervaala E, Muller DN, Gross V, Schmidt F, Park JK *et al*. Hypertension-induced end-organ damage: a new transgenic approach to an old problem. *Hypertension* 1999; **33**: 212–218.
9 Rodriguez-Iturbe B, Zhan CD, Quiroz Y, Sindhu RK, Vaziri ND. Antioxidant-rich diet relieves hypertension and reduces renal immune infiltration in spontaneously hypertensive rats. *Hypertension* 2003; **41**: 341–346.
10 Dorffel Y, Latsch C, Stuhlmuller B, Schreiber S, Scholze S, Burmester GR *et al*. Preactivated peripheral blood monocytes in patients with essential hypertension. *Hypertension* 1999; **34**: 113–117.
11 Ohki R, Yamamoto K, Mano H, Lee RT, Ikeda U, Shimada K. Identification of mechanically induced genes in human monocytic cells by DNA microarrays. *J Hypertens* 2002; **20**: 685–691.
12 Frohlich ED. Arthus C. Corcoran memorial lecture. Influence of nitric oxide and angiotensin II on renal involvement in hypertension. *Hypertension* 1997; **29**: 188–193.

13 Mun KC, Delano FA, Tran ED, Schmid-Schonbein GW. Microvascular cell death in spontaneously hypertensive rats during experimental inflammation. *Microcirculation* 2002; **9**: 397–405.
14 Suematsu M, Suzuki H, Delano FA, Schmid-Schonbein GW. The inflammatory aspect of the microcirculation in hypertension: oxidative stress, leukocytes/endothelial interaction, apoptosis. *Microcirculation* 2002; **9**: 259–276.
15 Robbins PD, Ghivizzani SC. Viral vectors for gene therapy. *Pharmacol Ther* 1998; **80**: 35–47.
16 Okada T, Shimazaki K, Nomoto T, Matsushita T, Mizukami H, Urabe M *et al*. Adeno-associated viral vector-mediated gene therapy of ischemia-induced neuronal death. *Methods Enzymol* 2002; **346**: 378–393.
17 Grimm D, Kay MA. From virus evolution to vector revolution: use of naturally occurring serotypes of adeno-associated virus (AAV) as novel vectors for human gene therapy. *Curr Gene Ther* 2003; **3**: 281–304.
18 Okada T, Nomoto T, Shimazaki K, Lijun W, Lu Y, Matsushita T *et al*. Adeno-associated virus vectors for gene transfer to the brain. *Methods* 2002; **28**: 237–247.
19 Rabinowitz JE, Rolling F, Li C, Conrath H, Xiao W, Xiao X *et al*. Cross-packaging of a single adeno-associated virus (AAV) type 2 vector genome into multiple AAV serotypes enables transduction with broad specificity. *J Virol* 2002; **76**: 791–801.
20 Hauck B, Xiao W. Characterization of tissue tropism determinants of adeno-associated virus type 1. *J Virol* 2003; **77**: 2768–2774.
21 Lammie GA. Hypertensive cerebral small vessel disease and stroke. *Brain Pathol* 2002; **12**: 358–370.
22 Kimura S, Saito H, Minami M, Togashi H, Nakamura N, Nemoto M *et al*. Pathogenesis of vascular dementia in stroke-prone spontaneously hypertensive rats. *Toxicology* 2000; **153**: 167–178.
23 Li L, Elliott JF, Mosmann TR. IL-10 inhibits cytokine production, vascular leakage, and swelling during T helper 1 cell-induced delayed-type hypersensitivity. *J Immunol* 1994; **153**: 3967–3978.
24 Silvestre JS, Mallat Z, Tamarat R, Duriez M, Tedgui A, Levy BI. Regulation of matrix metalloproteinase activity in ischemic tissue by interleukin-10: role in ischemia-induced angiogenesis. *Circ Res* 2001; **89**: 259–264.
25 Mostafa Mtairag E, Chollet-Martin S, Oudghiri M, Laquay N, Jacob MP, Michel JB *et al*. Effects of interleukin-10 on monocyte/endothelial cell adhesion and MMP-9/TIMP-1 secretion. *Cardiovasc Res* 2001; **49**: 882–890.
26 Mazighi M, Pelle A, Gonzalez W, Mtairag el M, Philippe M, Henin D *et al*. IL-10 inhibits vascular smooth muscle cell activation *in vitro* and *in vivo*. *Am J Physiol Heart Circ Physiol* 2004; **287**: H866–H871.
27 Cattaruzza M, Slodowski W, Stojakovic M, Krzesz R, Hecker M. Interleukin-10 induction of nitric-oxide synthase expression attenuates CD40-mediated interleukin-12 synthesis in human endothelial cells. *J Biol Chem* 2003; **278**: 37874–37880.
28 Henke PK, DeBrunye LA, Strieter RM, Bromberg JS, Prince M, Kadell AM *et al*. Viral IL-10 gene transfer decreases inflammation and cell adhesion molecule expression in a rat model of venous thrombosis. *J Immunol* 2000; **164**: 2131–2141.
29 Wang P, Wu P, Siegel MI, Egan RW, Billah MM. Interleukin (IL)-10 inhibits nuclear factor kappa B (NF kappa B) activation in human monocytes. IL-10 and IL-4 suppress cytokine synthesis by different mechanisms. *J Biol Chem* 1995; **270**: 9558–9563.
30 Ruiz-Ortega M, Bustos C, Hernandez-Presa MA, Lorenzo O, Plaza JJ, Egido J. Angiotensin II participates in mononuclear cell recruitment in experimental immune complex nephritis through nuclear factor-kappa B activation and monocyte chemoattractant protein-1 synthesis. *J Immunol* 1998; **161**: 430–439.
31 Lockyer JM, Colladay JS, Alperin-Lea WL, Hammond T, Buda AJ. Inhibition of nuclear factor-kappaB-mediated adhesion molecule expression in human endothelial cells. *Circ Res* 1998; **82**: 314–320.
32 Nava M, Quiroz Y, Vaziri N, Rodriguez-Iturbe B. Melatonin reduces renal interstitial inflammation and improves hypertension in spontaneously hypertensive rats. *Am J Physiol Renal Physiol* 2003; **284**: F447–F454.
33 Lentsch AB, Shanley TP, Sarma V, Ward PA. *In vivo* suppression of NF-kappa B and preservation of I kappa B alpha by interleukin-10 and interleukin-13. *J Clin Invest* 1997; **100**: 2443–2448.
34 Border WA, Noble NA. Interactions of transforming growth factor-beta and angiotensin II in renal fibrosis. *Hypertension* 1998; **31**: 181–188.
35 Gibbons GH, Dzau VJ. The emerging concept of vascular remodeling. *N Engl J Med* 1994; **330**: 1431–1438.
36 Kurihara H, Yoshizumi M, Sugiyama T, Takaku F, Yanagisawa M, Masaki T *et al*. Transforming growth factor-beta stimulates the expression of endothelin mRNA by vascular endothelial cells. *Biochem Biophys Res Commun* 1989; **159**: 1435–1440.
37 O'Callaghan CJ, Williams B. Mechanical strain-induced extracellular matrix production by human vascular smooth muscle cells: role of TGF-beta(1). *Hypertension* 2000; **36**: 319–324.
38 Dahly AJ, Hoagland KM, Flasch AK, Jha S, Ledbetter SR, Roman RJ. Antihypertensive effects of chronic anti-TGF-beta antibody therapy in Dahl S rats. *Am J Physiol Regul Integr Comp Physiol* 2002; **283**: R757–R767.
39 Hamaguchi A, Kim S, Ohta K, Yagi K, Yukimura T, Miura K *et al*. Transforming growth factor-beta 1 expression and phenotypic modulation in the kidney of hypertensive rats. *Hypertension* 1995; **26**: 199–207.
40 Manotham K, Tanaka T, Matsumoto M, Ohse T, Inagi R, Miyata T *et al*. Transdifferentiation of cultured tubular cells induced by hypoxia. *Kidney Int* 2004; **65**: 871–880.
41 Matsushita T, Elliger S, Elliger C, Podsakoff G, Villarreal L, Kurtzman GJ *et al*. Adeno-associated virus vectors can be efficiently produced without helper virus. *Gene Therapy* 1998; **5**: 938–945.
42 Nagaoka A, Kakihana M, Fujiwara K. Effects of idebenone on neurological deficits following cerebrovascular lesions in stroke-prone spontaneously hypertensive rats. *Arch Gerontol Geriatr* 1989; **8**: 203–212.

ELSEVIER

Experimental Hematology

Experimental Hematology 36 (2008) 37–50

Mutated D4-guanine diphosphate–dissociation inhibitor is found in human leukemic cells and promotes leukemic cell invasion

Yuji Nakata[a,b,d], Kensuke Kondoh[a,b,e], Sachiko Fukushima[a], Akinori Hashiguchi[a], Wenlin Du[a], Mutsumi Hayashi[a,b], Jun-ichiroh Fujimoto[c], Jun-ichi Hata[a,c], and Taketo Yamada[a]

[a]*Department of Pathology and* [b]*Department of Pediatrics, Keio University School of Medicine, Tokyo, Japan;* [c]*National Center for Child Health and Development, Tokyo, Japan;* [d]*Department of Medicine, Division Hematology/Oncology, University of Pennsylvania, Philadelphia, Pa., USA;* [e]*Department of Pediatrics, St. Marianna University School of Medicine, Kanagawa, Japan*

(Received 20 December 2006; revised 23 July 2007; accepted 13 August 2007)

Objective. **Rho GTPase may be involved in human cancer invasion via the augmentation of cell motility and adhesion. We report on two point mutations of the D4-guanine diphosphate (GDP)–dissociation inhibitor (GDI) gene, one of the Rho-GDIs, which were found in a human leukemic cell line, Reh, and the mutated D4-GDI functions as an accelerator of leukemic cell invasion.**

Material and Methods. **We investigated the altered activity of GDP dissociation by mutated (mt) D4-GDI and the functions of this mt and wild-type (wt) D4-GDI in invasion. The mice inoculated with wt or mt D4-GDI vector–transfected Raji cells were observed and examined pathologically. Adhesiveness and cell motility of wt or mt D4-GDI vector–transfected Raji cells were examined. Finally, it was examined whether Rho activation was changed by mutation of D4-GDI under the condition of Rho-GDI knockdown.**

Results. **Two point mutations of the D4-GDI gene were found in Reh cells. The region of mutations is conserved among members of the Rho-GDI family at the amino acid level. D4-GDI with two mutations (V68L and V69A) functioned in a dominant negative manner in the inhibition of GDP dissociation from Rho. Severe combined immune-deficient mice inoculated with Raji cells developed hemiparalysis. The Raji cells were present in bone marrow and peripheral blood, and hepatic invasion was observed in 20% of the mice. Mice inoculated with wt D4-GDI vector–transfected Raji cells (wt D4) showed later paralysis and none developed hepatic invasion. Mice inoculated with mt D4-GDI–transfected Raji cells (mt D4) showed a 5-day reduction in the time to paraplegia and death. In addition, hepatic invasion was evident in 80% of mice transplanted with mt D4 cells. There were no differences in growth rates and amounts of guanine triphosphate (GTP)–bound Rho, cdc42, or Rac among all clones, however, GTP-bound Rho in mt D4 clone with short hairpin RNA (shRNA) vector for Rho-GDI knockdown was increased compared with wt D4 clone with shRNA vector for Rho-GDI knockdown. The mt D4 cells showed an augmentation of adhesiveness and cell motility. On the other hand, wt D4 cells showed a decreased ability of cell motility.**

Conclusion. **These results suggest the mutated D4-GDI functions as a dominant negative molecule against the wt D4-GDI and accelerates invasion via regulation of cytoskeletal machinery.** © 2008 ISEH - Society for Hematology and Stem Cells. Published by Elsevier Inc.

Human leukemia progression is a process by which leukemic cells acquire more malignant properties, such as invasiveness. We previously established in vivo experimental systems of human leukemia invasion using severe combined immune-deficient (SCID) mice and reported that Rho activation augmented human leukemic cells invasion and changed the pattern of organs targeted by leukemic cells through the acceleration of leukemic cell adhesion [1].

The Rho, Rac, and Cdc 42 GTPases belong to the small guanine triphosphate (GTP)–binding protein family, a part of the Ras superfamily, and regulate various actin filament–dependent cell functions, such as cell adhesion, cell

Dr. Fukushima's current address: Department of Dermatology, Kanazawa University School of Medicine, Kanazawa, Japan.

Offprint requests to: Taketo Yamada, M.D., Department of Pathology, Keio University School of Medicine, 35 Shinano-machi, Shinjuku-ku, Tokyo 160-8582, Japan; E-mail: taketo@sc.itc.keio.ac.jp

0301-472X/08 $–see front matter. Copyright © 2008 ISEH - Society for Hematology and Stem Cells. Published by Elsevier Inc.
doi: 10.1016/j.exphem.2007.08.023

motility, and cytokinesis [2–5], as well as certain gene expressions [6]. These GTPases are active only in GTP-bound states and the exchange of GTP and guanine diphosphate (GDP) is strictly regulated by three types of regulatory proteins; GDP dissociation stimulators (GDS), GDP dissociation inhibitors (GDI), and GTPase activating proteins (GAP). Some GDS and GAP from the Rho family and three Rho GDIs have been isolated [7]. D4-GDI, one of the Rho GDIs, is preferentially expressed in hematopoietic cells, and Rho-GDIγ is expressed in the brain, lungs, kidneys, testes, and pancreas, while Rho-GDI is ubiquitously expressed in all mammalian organs [8–10]. Rho-GDI binds the majority of Rho-family GTPases in the cytoplasm, maintaining Rho in an inactive form in which it cannot interact with effecter targets or other regulatory proteins [11]. On the other hand, Rho-GDI also associated weakly with the GTP-bound forms of Rho, Rac, and Cdc42 [12,13]. This weak interaction resulted in an inhibition of the intrinsic and GAP-stimulated GTPase activities of the Rho GTPases. Thus, Rho-GDI appears to be a molecule capable of blocking the GTP binding/GTPase cycle at two points: at the GDP–GTP exchange step and the GTP hydrolytic step. Further studies demonstrated that Rho-GDI associates with a Rho-GDI displacement factor from the ERM family, which consists of ezrin, radixin, and moesin. ERM interacts with both an adhesion molecule—CD44—and F-actin, resulting in association of the actin cytoskeleton with the plasma membrane [14]. D4-GDI has been identified as a Rho-GDI–like protein that is approximately 68% homologous with Rho-GDI, and is preferentially expressed at very high levels in hematopoietic cells, including erythroid, granulocytic, monocytic, and lymphoid cells [8]. In another report, expression of D4-GDI in lymphocytes was emphasized and D4-GDI was named Ly-GDI [9]. The inhibitory effect of D4-GDI on GDP dissociation was specific for Rho, but not Ras or Rap [8]. Like other Rho-GDIs, D4-GDI was postulated to bind and inhibit Rho GTPases. However, much yet remains to characterize the specificity of D4-GDI [15,16].

D4-GDI has been reported to be a substrate of the apoptosis protease CPP32. D4-GDI was rapidly truncated to a 23-kDa fragment in Jurkat cells with kinetics that parallel the onset of apoptosis following Fas cross-linking with agonistic antibody or treatment with staurosporine [17]. Furthermore, Krieser et al. [18] showed that a cleaved 26-kDa fragment derived from D4-GDI resided in the cytoplasm of undamaged cells, whereas after cleavage by CPP32, the 22-kDa form of D4-GDI translocated to the nucleus [18]. These lines of evidence suggest that D4-GDI is involved in cell-shape alterations and/or changes in cell fragmentation during leukocyte apoptosis.

A number of Ras gene mutations have been found in a wide variety of human malignant tumors, including leukemias and lymphomas [19]. Point mutations in Ras cause decreased GTPase activity and may transform in some leukemic cells. Rho, a member of the Ras family, has not been associated with transformation, and no Rho mutations have been detected in human malignant tumors to date [20]. However, it has been reported that some regulatory proteins for Rho GTPases, dbl, tiam1, and vav, are reportedly associated with tumor development [7,21,22]. The Dbl oncogene was originally discovered because of its ability to induce focus formation and tumorigenicity when expressed in NIH-3T3 cells [23]. Tiam, however, was first identified as an invasion-inducing gene using proviral tagging in combination with in vitro selection for invasiveness [24]. Furthermore, the Rho family of small GTPases, including Rac, Cdc42, and Rho, has been implicated in the regulation of many aspects of cancer cell motility and invasion, including cell polarity, cytoskeletal organization, and transduction of signals from the extracellular environment [25–28].

In this study, we identified two point mutations of the D4-GDI gene in a human B-cell leukemia cell line, Reh, and analyzed the functions of the mutated (mt) D4-GDI in vitro and in vivo employing an experimental system consisting of human leukemic cell invasion in SCID mice.

Materials and methods

Human leukemic cells and cell culture

Two acute lymphoblastic leukemia cell lines (Reh and HPB-ALL) and three Burkitt's lymphoma cell lines (Raji [ATCC, CCL-86], Ramos [ATCC, CRL-1923], and Daudi [ATCC, CCL-213]) were examined. The Reh cell line was established from a girl with a common form of acute lymphoblastic leukemia [29]. This cell line is known to be accompanied by the TEL-AML1 fusion gene due to chromosomal translocation [30]. We used reverse transcriptase polymerase chain reaction (RT-PCR) to confirm that our Reh cells expressed mRNA derived from the TEL-AML1 fusion gene (data not shown). The Raji cell line was derived from Burkitt's lymphoma. The HPB-ALL cell line was derived from a pediatric T-cell leukemia [31]. Cells were cultured in the presence of 5% CO_2 at 37°C using RPMI-1640 medium supplemented with 10% fetal bovine serum. Normal human peripheral blood lymphocytes from healthy Japanese men were also examined with informed consent.

RT-PCR and DNA sequencing

Total RNA was extracted from each sample ($5–10 \times 10^6$ cells) using ISOGEN (Nippon Gene, Toyama, Japan). RNA was reverse-transcribed into first strand cDNA using a First-Strand cDNA Synthesis Kit (Amersham-Pharmacia Biotech, Buckinghamshire, UK). D4-GDI cDNA was isolated by PCR amplification from first-strand cDNA using the N-terminal primer (5′-TAAATA GATCAGAATGACTGAA-3′) and the C-terminal primer (5′-AGAATTCTTCCA AGGTGGCAA-3′). PCR was performed in 10 mM Tris-HCl (pH 9.0), 2.0 mM $MgCl_2$, 50 mM KCl, 0.2 mM each deoxyribonucleoside triphosphate, and 0.5 μM each PCR primer using Taq DNA Polymerase (Toyobo, Tokyo, Japan). Thirty cycles were run with denaturation at 94°C for 60 seconds, annealing at 55°C for 60 seconds, and extension at 72°C for 60

seconds. RT-PCR products were cloned into a pGEM-T vector (Promega, Madison, WI, USA), and analyzed with a Thermo Sequenase fluorescent–labeled primer cycle sequencing kit (Amersham-Pharmacia Biotech) using T7 and Sp6 fluorescent primer and a DNA sequencer (MegaBase 1000, Molecular Dynamics, Sunnyvale, CA, USA). The fluorescent primers used for sequencing were forward, 5′-GTCGCAGGAA ATGGACA AAGAT-3′ and reverse 5′-TCCAGTAA GGTCCATG GTGATT-3′.

Sequences of genomic D4-GDI DNA

DNA was prepared from Reh cells by standard methods with sodium dodecyl sulfate–proteinase K [32]. A portion of the D4-GDI gene that included the mutations was amplified using the N-terminal primer (5′-CACCACAGAAGTCCCTGAAAGA-3′) and the C-terminal primer (5′-TCCA GTAAGGTCCATGGT GATT-3′). PCR products were cloned into a pGEM-T vector and sequenced. After partial sequencing of the D4-GDI intron (data not shown), PCR products were analyzed by direct sequencing methods using the fluorescent forward primer (5′-CACCCAC TATACACATGTCTCT-3′) for the D4-GDI gene intron. Reh cells were also obtained from other laboratories and the D4-GDI gene was sequenced by the following method in order to eliminate any contamination of cells and to confirm the mutations. RT-PCR was performed with another N-terminal primer (5′-ACAGA GACGTGAAGCACTGAA-3′) and C-terminal primer (5′-GATG CATCAA TAAGGAAATGT-3′). These primers flanked the initial primers and were used to exclude contamination of PCR products and plasmids. PCR products were analyzed by direct sequencing method.

Construction of mt and wild-type D4-GDI expression vectors and short hairpin RNA vector for knockdown of Rho-GDI–α

Mutated D4-GDI cDNA of Reh cells was generated by RT-PCR. Wild-type (wt) D4-GDI cDNA was generated from HPB-ALL cells by RT-PCR. Vectors containing wt or mt D4-GDI cDNA with a myc-tag driven by the SRα promoter were constructed. This vector contained the neomycin-resistance (neo^r) gene driven by the SV40 promoter. The specific sequences for Rho-GDI small interfering RNA were searched by siDirect online software (RNAi Corporation, Tokyo, Japan). As a result, nucleotide number of human Rho-GDI–α 1191–1213 (3′UTR TCGGTCCCGTCTAAC CATGATGC) as Rho-GDI–α and scramble 23-nucleotide as control were generated. DNA-based small interfering RNA vectors were constructed in pBLOCK-iT6 DEST vector (Invitrogen, Carlsbad, CA, USA) for short hairpin RNA (shRNA) synthesis.

Transfection of wt or mt D4-GDI gene and shRNA vector for Rho-GDI knockdown into Raji cells

Wild-type or mt D4-GDI expression vector or shRNA vector for Rho-GDI knockdown was transfected into Raji cells by electroporation using a Gene Pulser (Bio-Rad, Hercules, CA, USA). The SRα–myc-tag vector or shRNA vector with scramble 23-nucleotide was transfected into Raji cells as a control. The Raji cells were cultured in culture media with G418 (800 μg/mL; Sigma-Aldrich, Tokyo, Japan) or blasticidin (10 μg/mL; Invitrogen, Carlsbad, CA, USA) for 14 days, followed by subcloning in a 96-well plate twice. Expression of D4-GDI or Rho-GDI–α protein was confirmed by Western blotting using a rabbit anti–D4-GDI or Rho-GDI polyclonal antibody (Zymed Laboratory, San Francisco, CA, USA). Blotted membranes were treated with peroxidase-conjugated anti-rabbit immunoglobulin antibody and visualized with electrochemiluminescence (Amersham-Pharmacia Biotech). The protein concentration was measured by BCA protein assay reagent (Pierce, Rockford, IL, USA).

Transplantation of leukemic cells into SCID mice

SCID mice (C.B.17 SCID mice, female, 7 to 9 weeks after birth; Clea, Tokyo, Japan) were maintained under specific pathogen-free conditions, and 2×10^7 Raji cells with/without wt or mt D4-GDI or Rho-GDI shRNA were suspended in 100 μL culture medium and injected into the tail veins of mice.

Analysis of leukemic cell invasion in SCID mice

Development of hemiparalysis in the mice was defined as the state in which they showed no motion of their hemilateral lower extremities. On day 17 or 20, when all mice were still alive and some showed hemiparalysis, the mice were sacrificed. Peripheral blood was prepared from the orbital vein plexus and cells were taken from the bilateral femurs and tibiae, and the spleen. The peripheral blood was subjected to hemolysis before being washed in phosphate-buffered saline (pH 7.4). Samples were then subjected to staining with anti-human CD19 monoclonal antibody (phycoerythrin-conjugated; DAKO, Glostrup, Denmark, diluted 1:100) for analysis with a flow cytometer (EPICS XL-MCL; Beckman Coulter, Hialeah, FL, USA). The systemic organs of mice were also prepared for pathological analysis by fixation in 10% formaldehyde in phosphate-buffered saline, embedding in paraffin, sectioned and then stained with hematoxylin-eosin. Immunohistochemical analyses were performed with anti-human CD19 monoclonal antibody and anti-proliferating cell nuclear antigen (PCNA) monoclonal antibody (Oncogene Science, Uniondale, NY, USA, diluted 1:50).

In vitro and in vivo proliferation assay

Proliferation rates of Raji cells with mt or wt D4-GDI or myc-tag only and shRNA vector for Rho-GDI knockdown or scramble 23-nucleotide were determined using the MTT method. These three clones were placed in eight wells of a round-bottomed 96-well plate at a concentration of 2×10^3 cells/100 μΛ/well and cultured for 48 hours, followed by addition of 5 mg/mL MTT (3-[4,5-dimethylthiazol-2-yl]-2,5-diphenyltetrazolium bromide; Sigma-Aldrich) at a concentration of 10 μL/well and further cultured for 4 hours. After the cells had settled on the plate, 100 μL 0.04 N HCl plus isopropanol was added. The resultant mixture was stirred and then measured using an enzyme-linked immunosorbent assay reader (Microplate Reader Model 450; Bio-Rad) for absorbance at 570 nm and 630 nm.

The in vivo proliferative capabilities of leukemic cells were investigated by the PCNA labeling index in situ [33]. The number of nuclear PCNA-positive cells and total cells in the vertebrae were counted in 10 fields.

Cell motility assay

Cell migration ability was assessed in 48-well chambers using polyvinylpyrrolidone-free polycarbonate membranes with 5-μm or 3-μm pores (NeuroProbe, Inc., Gaithersburg, MD, USA). RPMI-1640 supplemented with 1% pasteurized human plasma was placed in lower wells, and used to dilute the cells in upper wells. After 3 hours at 37°C, the membrane was removed, washed on the upper side with phosphate-buffered saline, then fixed and stained with DiffQuik (NeuroProbe). All assays were done in triplicate, and migrated cells were counted in five randomly selected

fields at 600-fold magnification. General and spontaneous migration was determined in the absence of chemokines.

Adhesion assays

Adhesion of Raji cells to the extracellular matrix or cells was assessed. Extracellular matrices (Matrigel; Becton-Dickinson, Mountain View, CA, USA), human fibronectin, laminin, and collagen type IV (Asahi Techno Glass, Funabashi, Chiba, Japan) were used in the 24-well Biocoat cellware (Becton-Dickinson). Human bone marrow stromal cells, which were obtained from bone marrow specimens of nonhematological patients, with informed consent, were seeded in 24-well plates prior to 24-hour adhesion assays. Cells were fluorescently labeled with 2 μM 2,7-bis-(2-carboxyethyl)-5 (and 6) carboxyfluorescein (BCECF; Molecular Probes, Eugene, OR, USA) for 30 minutes at 37°C. Labeled cells were washed twice, resuspended with RPMI to achieve a concentration of 2×10^5 cells/mL, and added to each well. After incubation with fixative, plates were washed and the number of fluorescent cells bound was determined by proportionality to the remaining BCECF fluorescence measured using a FluorImager 595 (Molecular Dynamics).

Affinity-precipitation of cellular GTP-bound Rho, Cdc42, and Rac

Ren et al. [34] developed a method based on evidence that Rho effectors interact only with GTP-bound Rho for the measurement of Rho activity [34]. Binding of Rho to the Rho-binding domain (RBD) from the effector protein Rhotekin inhibited both the intrinsic and GAP-enhanced GTPase activity of Rho [35]. Therefore, Rhotekin RBD was used to affinity-precipitate cellular GTP-Rho. Cells were washed with ice-cold Tris-buffered saline and lysed in RIPA buffer (50 mM Tris [pH 7.2], 1% Triton X-100, 0.5% sodium deoxycholate, 0.1% sodium dodecyl sulfate, 500 mM NaCl, 10 mM $MgCl_2$, 10 mg/mL each of leupeptin and aprotinin, and 1 mM phenylmethylsulfonyl fluoride). Cell lysates were clarified by centrifugation at 13,000*g* at 4°C for 10 minutes, and equal volumes of lysates were incubated with GST-RBD (a fusion of RBD with glutathione S-transferase, 20 μg) beads at 4°C for 45 minutes. Beads were washed four times with buffer B (Tris buffer containing 1% Triton X-100, 150 mM NaCl, 10 mM $MgCl_2$, 10 mg/mL each of leupeptin and aprotinin, and 0.1 mM phenylmethylsulfonyl fluoride). Bound Rho proteins were detected by Western blotting using an anti-RhoA monoclonal antibody (Santa Cruz Biotechnology, Santa Cruz, CA, USA). Densitometric analysis was performed using NIH image version 1.62. The amount of RBD-bound Rho was normalized to the total amount of Rho in cell lysates for the comparison of Rho activity (level of GTP-bound Rho) in different samples. Depending on cell conditions and types, and different batches of GST-RBD, the RBD-bound Rho accounts for ~0.5% to 5% of total Rho. The measurement of Rac activity was performed using the Rac Activation Assay kit (Cytoskeleton, Denver, CO, USA) according to the manufacturer's protocol.

[^{3}H]GDP dissociation assay

D4-GDI (wt, V68L, V69A, and both V68L and V69A mutations) protein was synthesized using Baculo-viral expression system with Bac-to-Bac HT vector (Invitrogen, Carlsbad, CA, USA) and Sf9 cells. His-tag D4-GDI proteins in cell lysates were purified using Ni-NTA agarose and ProBond Purification system (Invitrogen) according to the manufacturer's protocol. The inhibitory activities of wt, mt (V68L, V69A, and both V68L and V69A mutations), and wt plus each mt D4-GDI on GDP dissociation from isoprenylated Rho were determined using a filtration assay, as described previously by Chuang et al. [13]

Statistical analysis

All results were evaluated using Student's *t*-test–based statistics. Experiments were performed at least three times each.

Results

Detection of mutations of D4-GDI cDNA or genomic DNA in human leukemic cells

Results of DNA sequence analysis of the D4-GDI cDNA from the human leukemic cell lines are shown in Figure 1. Two point mutations at positions 276 (a G to C change) and 280 (T to C) were found in the D4-GDI cDNA of the Reh cell line. No mutations of the D4-GDI gene were detected in the D4-GDI genes of HPB-ALL, Raji, Ramos, and Daudi cell lines or in normal human peripheral blood lymphocytes (data not shown). Direct sequencing analysis of genomic DNA showed that these mutations were present on one allele (Fig. 2). These two point mutations of D4-GDI in the Reh cell led to conversions of valine 68 to leucine and valine 69 to alanine. The alignment of the predicted amino acid sequences of mt D4-GDI, wt D4-GDI, and other Rho-GDI family genes are shown in Figure 1. These two mutations exist in the partially conserved region at the amino acid level.

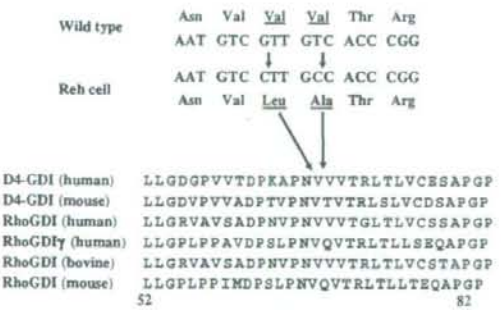

Figure 1. Two point mutations of D4-GDI cDNA in Reh cells and alignment of the predicted amino acid sequence. Two point mutations in D4-GDI were detected in Reh cells (arrows). These changes resulted in a guanine to cytosine substitution at position 276 and a thymine to cytosine substitution at nucleotide 280 (underlined). The alignment of predicted amino acid sequences of D4-GDI and Rho-GDI family genes. The two D4-GDI point mutations in Reh cells led to a valine 68 to leucine change and a valine 69 to alanine change. This region is highly conserved in Rho-GDI family members.

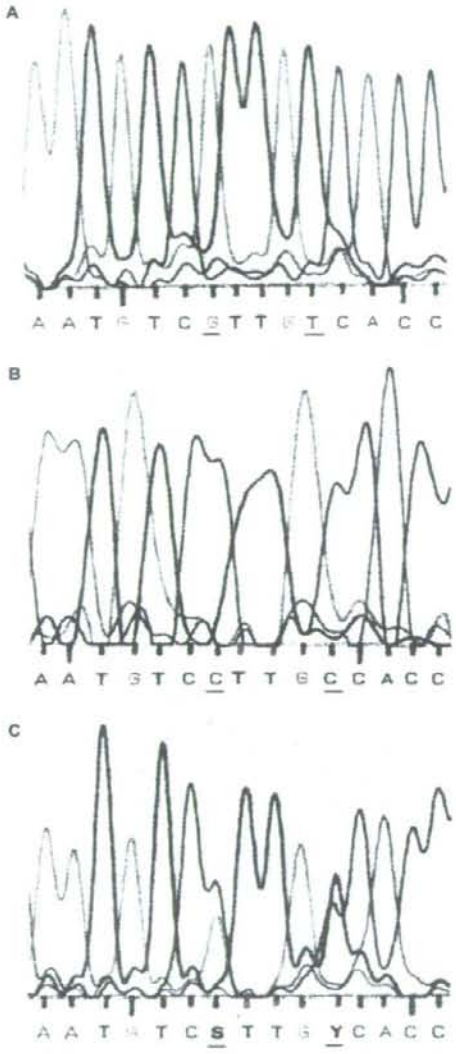

Figure 2. Heterozygous mutations of the D4-GDI gene in Reh cells. (**A**) Normal D4-GDI sequence from normal human peripheral blood lymphocytes. (**B**) Two point mutations in D4-GDI in Reh cells (underlined). These changes resulted in a guanine to cytosine substitution at position 276 and a thymine to cytosine substitution at nucleotide 280. (**C**) Direct sequence analysis of DNA amplified from genomic DNA of Reh cells showed identical mutations in one allele (heterozygous). Arrowheads indicate the two peaks, guanine and cytosine at position 276, and thymine and cytosine at nucleotide 280.

Gene transfer of wt or mt D4-GDI expression vector into Raji cells

A human leukemic cell line (Raji) was used in order to clarify the functions of mt or wt D4-GDI, because there were no mutations of D4-GDI gene in the Raji cells. Some clones with wt D4-GDI, mt D4-GDI, or the myc-tag vector were obtained and used in subsequent experiments. Expression of exogenous D4-GDI in these clones was confirmed by Western blotting using anti–D4-GDI polyclonal antibody. These cells expressed a protein of approximately 29 kDa, which was recognized by the D4-GDI antibody (Fig. 3A). The lower bands were endogenous D4-GDI in Raji cells and the upper bands were the exogenous D4-GDI with the myc-tag. We detected the expression of exogenous D4-GDI protein by Western blotting using anti-myc-tag antibody (9E10) (data not shown). The amounts of exogenous D4-GDI were almost the same as the endogenous D4-GDI in clones 21 and 26 with wt D4-GDI and in clone 13 with mt D4-GDI.

Gene transfer of a shRNA vector for Rho-GDI knockdown into Raji cell clones with wt or mt D4-GDI expression vector

The Raji cells with the wt D4-GDI (clone 3) or the mt D4-GDI (clone 13) were transferred with a shRNA vector for Rho-GDI knockdown or a vector of scramble shRNA as a control. Clones that were selected by blasticidin were examined by Western blotting using anti–Rho-GDI polyclonal antibody. Expression of Rho-GDI in clone wt3-21 and mt13-27 with Rho-GDI shRNA vector was decreased compared with clone wt3-1 and mt13-3 with scramble shRNA vector as a control (Fig. 3B). The clones with decreased expression under a quarter of Rho-GDI were established from the Raji cells with the wt D4-GDI, on the other hand, clones with a decreased expression under a half of Rho-GDI were not obtained from the Raji cells with the mt D4-GDI.

Exogenous D4-GDI expressions alter invasion of human leukemic cells in SCID mice

Wild-type D4-GDI clones (21 and 26), mt D4-GDI clones (13 and 20), and two myc-tag clones (1 and 4) were inoculated into SCID mice intravenously. The hemiparalysis and survival curves are summarized in Figure 4A. All mice (n = 18) inoculated with the myc-tag clone (as a control) developed hemiparalysis at 18 to 41 days (mean: 24 days) after transplantation. Histological analysis of systemic organs on day 20 revealed that the myc-tag clones invaded the liver in two of the nine mice (22%). Myc-tag clones were present in peripheral blood (3–52% of white blood cells) and bone marrow (3–66% of mononuclear cells) on day 20. Myc-tag clones infiltrated both ovaries, as well. There were no invasions of myc-tag clones into the brain, salivary glands, lungs, kidneys, digestive tract, heart, adrenal glands, spleen, or thymus. In the mice with hemiparalysis, numerous monotonous blasts occupied the bone marrow of vertebrae and femora, and also extended beyond the bone into the epidural space of the spinal cord, and into neighboring muscles (Fig. 5A). The murine hematopoiesis in bone marrow was markedly suppressed

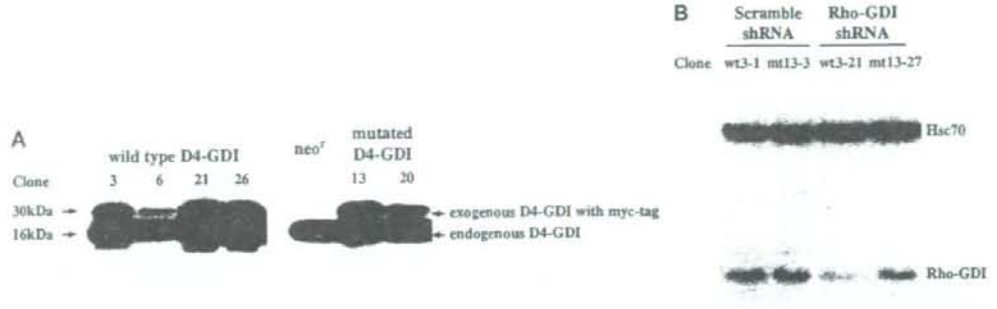

Figure 3. Gene transfer of wild-type or mutated D4-GDI expression vector into Raji cells and a vector of shRNA for Rho-GDI knockdown. (**A**) The Raji cells carrying the D4-GDI gene (clones 3, 6, 21, and 26 with wild-type D4-GDI vector and clone 13 and 20 with mutated D4-GDI vector) were prepared in Laemmeli's buffer and resolved by sodium dodecyl sulfate polyacrylamide gel electrophoresis. Western blotting was performed using anti-D4-GDI polyclonal antibody, peroxidase-conjugated secondary antibody, and electrochemiluminescence for visualization. The transfected cells expressed proteins of approximately 29 kDa and 30 kDa. The 29-kDa bands were endogenous D4-GDI and the upper bands were exogenous D4-GDI with myc tag. (**B**) The Raji cells with the wild-type (wt) D4-GDI (clone 3, wt3) or the mutated (mt) D4-GDI (clone 13, mt13) were transferred with a vector of shRNA for Rho-GDI knockdown. Selected clones were examined by Western blotting using anti-Rho-GDI polyclonal antibody. Expression of Rho-GDI in clone wt3-21 and mt13-27 with Rho-GDI shRNA vector was decreased compared with clone wt3-1 and mt13-3 with scramble shRNA vector as a control.

by infiltration of human leukemic cells. In addition, the spinal cord showed spongiosis, suggesting that development of hemiparalysis in these mice was attributable to invasion of the epidural space by leukemic cells (Fig. 5A). All mice inoculated with myc-tag clones died at 20 to 43 days posttransplantation.

Hemiparalysis in SCID mice inoculated with wt D4-GDI clones was apparently delayed as compared with the mice inoculated with myc-tag clones. These mice developed hemiparalysis (Fig. 4A). Eighteen of the 26 had hemiparalysis at 18 to 49 days (mean: 33.9 days, $p < 0.01$) after transplantation. Some of the SCID mice inoculated with wt D4-GDI clones developed hemiparalysis during the 60-day observation period (69% of all mice). The remaining mice survived more than 60 days (31% of all mice). There were no invasions of Raji cells with wt D4-GDI overexpression in the liver on day 20 after transplantation (0 of the 6 mice). The wt D4-GDI clones were present in peripheral blood (3–9% of white blood cells) and bone marrow (4–10% of white blood cells) on day 20.

On the other hand, SCID mice inoculated with mt D4-GDI clones began to develop hemiparalysis earlier, i.e., on day 14, after transplantation as compared with the mice inoculated with myc-tag clones, which developed similar paralysis after day 18 posttransplantation (Fig. 4A). All mice with mt D4-GDI ($n = 20$) developed hemiparalysis at 14 to 20 days (mean: 17.4 days, $p < 0.01$) after transplantation.

Histological analysis of mice inoculated with the mt D4-GDI clones revealed hepatic invasion of leukemic cells on day 17 in 8 of the 10 mice (80%), and all had larger invasive areas than the control myc-tag mice (Fig. 5B and C). Furthermore, invasions of Raji cells into the brain, kidneys, and ovaries in some of the mt D4-GDI clone–transplanted mice were found (date not shown). All mice died at 17 to 26 days posttransplantation.

The wt D4-GDI clones (wt3-1 or wt3-21) or mt D4-GDI clones (mt13-3 or mt3-27) with a vector for shRNA of Rho-GDI or a vector of scramble shRNA, respectively, were inoculated into SCID mice intravenously because the effect of mt D4-GDI in leukemic cell infiltration under the condition of decreased expression of Rho-GDI was examined. The hemiparalysis and survival curves are summarized in Figure 4B. The time course of development of hemiparalysis in SCID mice inoculated with wt3-1 clone was similar to mice inoculated with wt3-21 clone. Furthermore, hemiparalysis of mice inoculated with mt13-27 clone was not altered compared with the mice inoculated with mt13-3 clone as a control.

In vitro and in vivo cell proliferation

We examined whether the altered invasiveness of leukemic cells in vivo was attributable to certain changes in their proliferative abilities. However, MTT assay indicated that there were no differences in proliferation among wt D4-GDI clones, mt D4-GDI clones, and myc-tag clones in vitro (Fig. 6). An immunohistochemical analysis using anti-PCNA antibody was done in order to identify the proportion of in situ leukemic cells in S phase. PCNA is expressed in the nuclei of cells in the S phase in parallel with incorporation of bromodeoxyuridine or [^{3}H]-thymidine [1,33]. Almost all PCNA-positive cells in the bone marrow were human leukemic cells. There were no significant differences among the PCNA-labeling indices of wt D4-GDI clones, mt D4-GDI clones, and myc-tag clones (data not shown). These results indicate that neither wt nor mt D4-GDI expression altered leukemic cell invasion via induction of cell proliferation. The proliferating activity of the wt

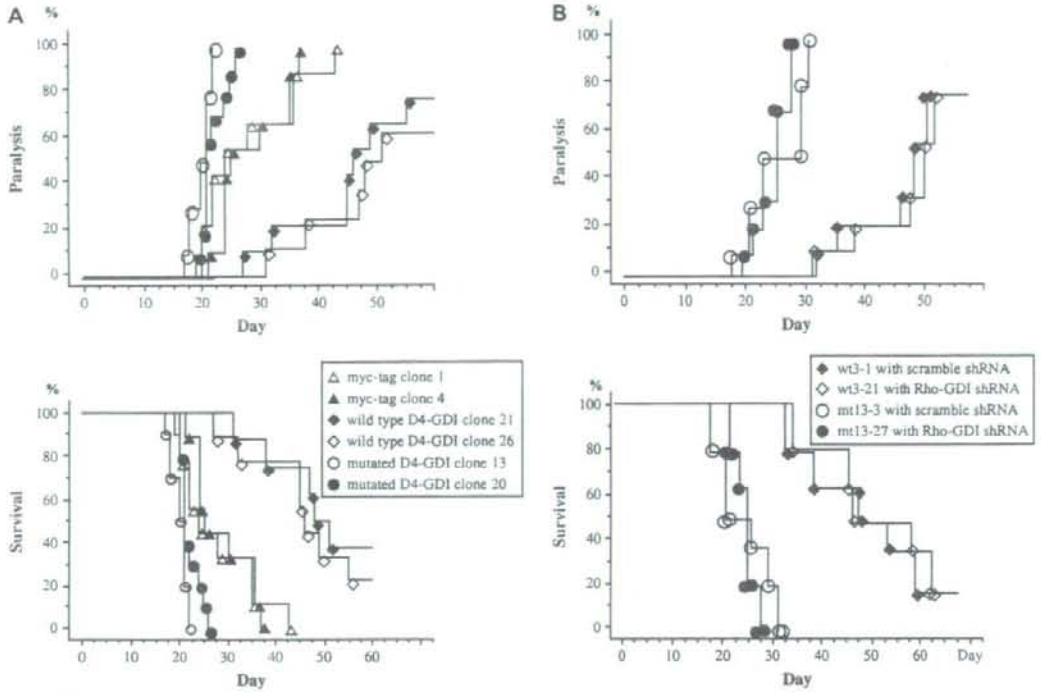

Figure 4. Alteration of hemiparalysis and survival with exogenous D4-GDI expressions in leukemic cells. (**A**) Hemiparalysis was observed in severe combined immune deficient (SCID) mice inoculated with wild-type D4-GDI clones (21 and 26), mutated D4-GDI clones (13 and 20) and myc-tag clones (1 and 4). The mice inoculated with wild-type D4-GDI clones developed hemiparalysis later than myc-tag clone–transplanted mice. On the other hand, the mutated D4-GDI clone–transplanted mice developed hemiparalysis earlier than the myc-tag clone–transplanted mice. Data on the appearance of hemiparalysis; Myc-tag clone transplanted mice (n = 18) at 18 to 41 days (mean: 24 days), wild-type D4-GDI–transplanted mice (n = 26) at 18 to 49 days (mean: 33.9 days, $p < 0.01$), and mutated D4-GDI–transplanted mice (n = 20) at 14 to 20 days (mean: 17.4 days, $p < 0.01$) after transplantation. (**B**) The wild-type D4-GDI clones (wt3-1 or wt3-21) or mutated D4-GDI clones (mt13-3 or mt3-27) with a vector for shRNA of Rho-GDI or a vector of scramble shRNA were inoculated into SCID mice. The hemiparalysis and survival curves are not altered. The time course of development of hemiparalysis in SCID mice inoculated with wt3-1 clone was similar to mice inoculated with wt3-21 clone. The hemiparalysis of mice inoculated with mt13-27 clone was not altered compared with the mice inoculated with mt13-3 clone as a control.

D4-GDI clones (wt3-1 or wt3-21) or mt D4-GDI clones (mt13-3 or mt3-27) with a vector for shRNA of Rho-GDI or a vector of scramble shRNA were examined using MTT assay in order to observe the function of mt D4-GDI under the condition of decreased expression of Rho-GDI. As a result, no differences between these clones (wt3-1, wt3-21, mt13-3 or mt3-27) were revealed (data not shown).

Alteration of cellular motile activity by exogenous D4-GDI expression

We attempted to estimate changes in general cell motility in response to exogenous D4-GDI expression in leukemic cells, because we did not detect differences in cell proliferation of wt or mt D4-GDI clones in vitro or in vivo. As a result, mt D4-GDI clones had increased cell motilities ($p < 0.001$), and wt D4-GDI clones had decreased cell motilities ($p < 0.01$) as compared with the myc-tag clones, without chemokines in vitro (Fig. 7). The cellular motile activities of each clone would correspond to the invasive activities (see Figs. 4 and 5). Mutated D4-GDI clone 13 showed the highest motile activity in vitro and the highest invasive activity in vivo. The motile activity of wt or mt D4-GDI clones (wt3-1, wt3-21, mt13-3, or mt3-27) with a vector of scramble shRNA or a vector for shRNA of Rho-GDI were examined in order to analyze the function of mt D4-GDI under the condition of decreased expression of Rho-GDI. As a result, no alterations between clone wt3-1 and wt3-21, or between clone mt13-3 and mt3-27, were observed (data not shown).

Augmentation of cell adhesion by mt D4-GDI expression

Cell motility consists of multiple and complex steps, including a response against chemotactic factors, cytoskeletal organization, and cell adhesion. We investigated whether exogenous D4-GDI expression altered the motile activity of leukemic cells through changes in cell adhesion. Adhesion of Raji cells, which contain mt or wt D4-GDI or the

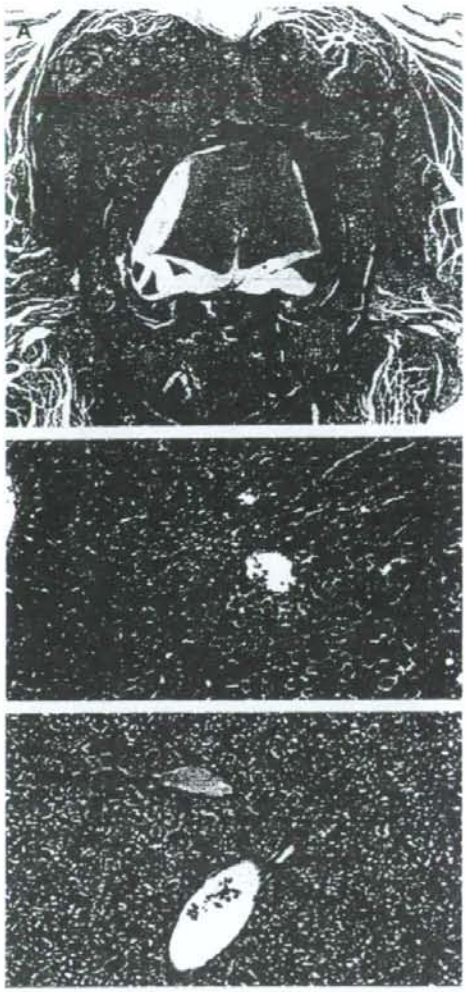

Figure 5. Raji cell invasion in severe combined immune deficient (SCID) mice. (**A**) The vertebra of an SCID mouse inoculated with myc-tag clone 1 is shown in a transverse section (hematoxylin-eosin staining). Raji cells have invaded the bone marrow, surrounding tissues, and the epidural space (day 17 after transplantation). The result is spongiosis, due to compression myelopathy of the spinal cord. S and L indicate the spinal cord and human leukemic (Raji) cells, respectively. Original magnification ×100. (**B**) Hepatic invasion by mutated D4-GDI clone 13 is shown. Original magnification ×120. (**C**) On other hand, there was no hepatic invasion in mice inoculated with wild-type D4-GDI clone 26. Original magnification ×120.

myc-tag only, to the extracellular matrix or cells was assessed as described previously [1]. Extracellular matrices (Matrigel [Becton-Dickinson], human fibronectin, laminin, and collagen type IV) were placed in 24-well dishes. In order to quantitate cell-adhesion activity, the leukemic cells were labeled with 2 μM BCECF, washed, and the fluorescence was then measured with a FluorImager 595. As a result, no significant differences in adhesiveness between these clones on each extracellular matrix (Matrigel, human fibronectin, laminin, and collagen type IV) were observed (data not shown). However, differences in adhesiveness to the stromal cells were obvious. In contrast to the myc-tag and wt D4-GDI clones, the mt D4-GDI clones showed augmented adhesiveness to human bone marrow stromal cells ($p < 0.05$) (Fig. 8). There was a significant difference in adhesion to human stromal cells between the myc-tag clones and the wt D4-GDI clones.

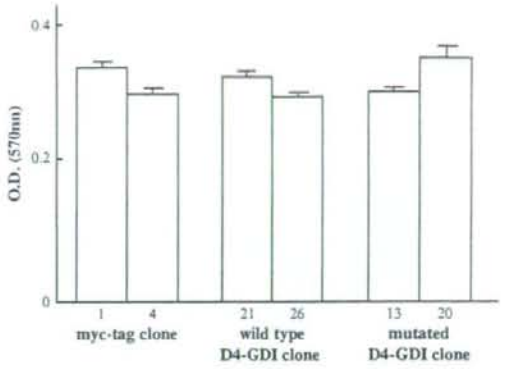

Figure 6. Exogenous D4-GDI expression does not change cell growth rates. The in vitro growth rates of myc-tag clones, wild-type D4-GDI clones, and mutated D4-GDI clones were compared by performing MTT assays. There were no significant differences in proliferative ability among these clones.

Cell-adhesion activity of wt or mt D4-GDI clones (wt3-1, wt3-21, mt13-3, or mt3-27) with a vector of scramble shRNA or a vector for shRNA of Rho-GDI was examined in order to analyze the function of mt D4-GDI under the condition of decreased expression of Rho-GDI. As a result, no differences in adhesion activity between clone wt3-1 and wt3-21, or between clone mt13-3 and mt3-27, were revealed (data not shown).

Detection of cellular GTP-bound Rho, Cdc42, and Rac in leukemic cells

We investigated whether D4-GDI (wt or mt) overexpression in leukemic cells altered Rho and Rac activity. We employed a pull-down assay using RBD affinity-precipitation and Western blotting with anti-RhoA antibody (see Materials and Methods). The proportions of activated Rho (GTP-bound Rho/total Rho) did not differ among myc-tag, wt D4-GDI, and mt D4-GDI clones (Fig. 9). GTP-bound Rho accounted for 1.3% to 1.6 % of total Rho in all experiments. In order to confirm the absence of differences in Rho activity among these clones, the immunoprecipitation with anti-RhoA antibody was carried out after metabolic pulse chase labeling with [^{35}S]-GTPγs. The uptakes of [^{35}S]-GTPγs into RhoA for 8 hours in myc-tag, wt D4-GDI, and mt D4-GDI clones were not different (data not shown). Furthermore, no differences of the

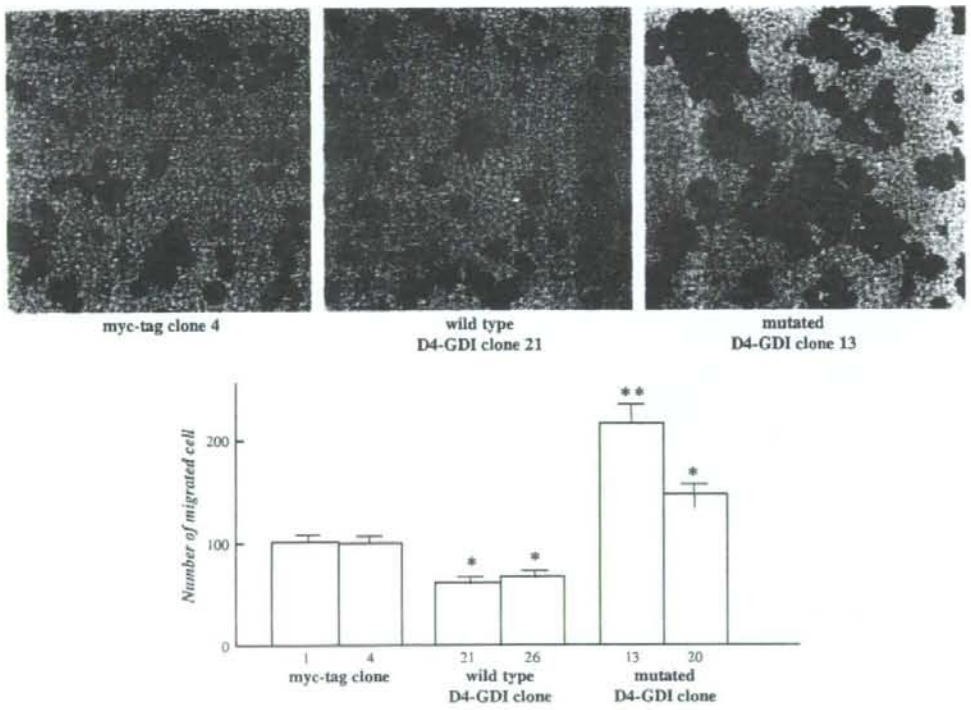

Figure 7. Alteration of cell motility by wild-type or mutated D4-GDI overexpression. The in vitro cellular motile activities of myc-tag clones, wild-type D4-GDI clones, and mutated D4-GDI clones were compared using a chemotaxis chamber (NueroProbe), without hemotactic factors (see Materials and Methods). In contrast to myc-tag clones 1 and 4, mutated D4-GDI clones 13 and 20 showed markedly increased motilities. On the other hand, wild-type D4-GDI clones 21 and 26 showed significantly decreased cell motilities. The upper colored figures show results representative of migrated leukemic cells stained with Diff-Quik (NeuroProbe). Data are represented as mean values. Error bars show standard error of mean. ** and * indicate statistically significant increases ($p < 0.001$ and $p < 0.01$, respectively) as compared to data from myc-tag clone 1 or 4.

Cdc42 and Rac activities between these clones were also observed (Fig. 9A).

Alterations of cellular GTP bound-Rho under the condition of decreased expression of Rho-GDI in leukemic cells with wt D4-GDI or mt D4-GDI overexpression were examined. The pull-down assay for Rho using the wt or mt D4-GDI clones (wt3-1, wt3-21, mt13-3, or mt3-27) with a vector of scramble shRNA or a vector for shRNA of Rho-GDI were done. As a result, the GTP-bound Rho in Rho-GDI knockdown clones (both wt3-21 and mt13-27) was slightly increased compared with clones with scramble shRNA vector (wt3-1 and mt13-3). Especially the difference of GTP-bound Rho/total Rho ratio between mt13-3 and mt13-27 was greater than the difference between wt3-1 and wt3-21. This dissimilarity between wt D4 clones and mt D4 clones in Rho activation by Rho-GDI knockdown may show that the mt D4-GDI proteins impair certain D4-GDI functions.

These results show the exogenous mt D4-GDI expression to be involved in the invasiveness of human leukemic cells through augmentation of cell motility and/or cell-adhesion activity. The altered phenotypes of leukemic cells may be caused by Rho activation due to the mt D4-GDI expression.

Mutated D4-GDI functioned in a dominant negative manner in the inhibition of GDP dissociation from Rho in vitro

While human D4-GDI has been previously shown to inhibit GDP dissociation from Rho family GTPases, we used purified recombinant proteins of wt and mt D4-GDI (V68L or V69A or both V68L and V69A) to directly compare their activities. Sf9 cell–expressed isoprenylated Rho were preloaded with [^{3}H]GDP, and the ability of wt D4-GDI, mt D4-GDIs, and wt plus mt D4-GDIs to inhibit dissociation of the nucleotide was determined. The dissociation of [^{3}H]GDP from Rho was totally blocked by wt D4-GDI (Fig. 10). The dissociation activity of [^{3}H]GDP from Rho by mt D4-GDI with both mutations of V68L and V69A was significantly low. On the other hand, the dissociation activity of mt D4-GDI with single mutation (V68L or V69A) was mild. Furthermore, inhibition of dissociation of [^{3}H]GDP

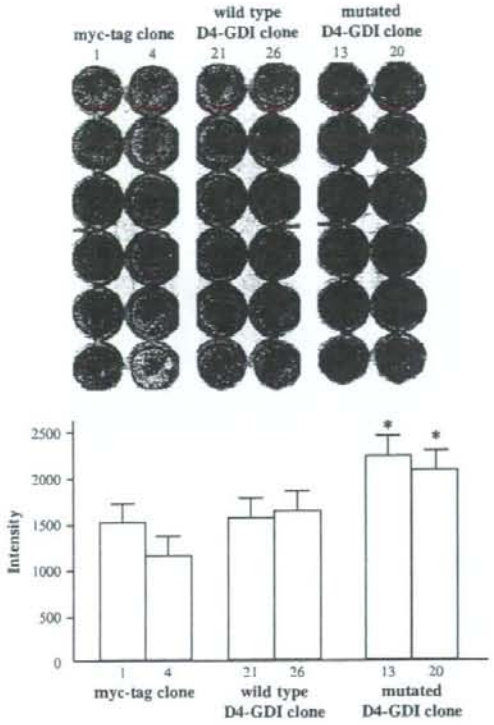

Figure 8. Augmentation of cell adhesion to human bone marrow stromal cells by mutated D4-GDI expression. The cell-adhesion activities of myc-tag clones, wild-type D4-GDI clones, and mutated D4-GDI clones were compared by using quantitative adhesion assays with fluorescent labeling of living cells (see Materials and Methods). In the upper panel, the unlabeled human stromal cells (invisible) attached to all wells and 2,7-bis-(2-carboxyethyl)-5 (and 6) carboxyfluorescein–labeled Raji cell clones, which adhered to the stromal cells were visible like black granules. The vertical line (six wells) represents data derived from one clone. In contrast to myc-tag clones 1 and 4, the mutated D4-GDI clones showed increased adhesiveness to human bone marrow stromal cells ($p < 0.05$). There was no significant difference in adhesion to human stromal cells between the myc-tag clones and wild-type D4-GDI clones. Data are represented as mean values. Error bars show standard error of mean. *Indicates a statistically significant increase ($p < 0.05$) as compared to data from myc-tag clone 1 or 4.

from Rho by wt D4-GDI was impaired by the addition of mt D4-GDI with both mutations of V68L and V69A. The negative effect by the addition of mt D4-GDI with single mutation of V68L or V69A to wt D4-GDI was not observed. As a result, the mt D4-GDI proteins with two mutations may function in a dominant negative manner in vitro.

Discussion

We identified two point mutations of D4-GDI in the human B-cell leukemic cell line. The region of D4-GDI containing these point mutations, which result in amino acid substitutions, is partially conserved in Rho-GDI family genes (Fig. 1). X-ray analysis of the three-dimensional structure of Rho-GDI suggested that these mutations of D4-GDI are in a β-sheet structure [36]. This region is at the back of the continuous surface adjacent to the isoprene-binding site of Rho-GDI, and could easily contact the bound GTPase and impart GDI activity. Robson protein secondary structure prediction suggested that these mutations may influence the β-sheet region [37]. The dissociation activity of GDP of D4-GDI with both mutations of V68L and V69A was decreased greater than the dissociation activity of mt D4-GDI with single mutation (V68L or V69A). Furthermore, dissociation of GDP from Rho by wt D4-GDI was significantly impaired by the addition of mt D4-GDI with both mutations of V68L and V69A. This result suggests that the D4-GDI proteins with two mutations may function in a dominant negative manner.

Thus, we speculated that this mt D4-GDI plays a role in development of hematological malignancy, and analyzed functions of mt D4-GDI in human leukemic cell invasion in vivo using a transplantation model of human leukemic cells into SCID mice. The SCID mice inoculated with Reh cells developed paraplegia 21 days after inoculation and all had died by days 26 to 27. The Reh cells infiltrated into bone marrow and around the spinal cord, with no involvement into peripheral blood, the spleen, liver, thymus or lymph nodes [1]. We identified mutations in the D4-GDI gene from human leukemic cells and showed that overexpression of mt D4-GDI in Raji cells accelerates leukemic cell invasion. Furthermore, we showed that overexpression of wt D4-GDI in Raji cells suppresses invasiveness. Additionally, there were no differences in cell growth rates among these clones, despite the altered invasiveness. On the other hand, cellular motile activity in the mt D4-GDI clones was augmented as compared with the myc-tag clones, and the motile activity of wt D4-GDI clones was significantly decreased. In the cell-adhesion assay, the mt D4-GDI clones showed increased adhesiveness to human bone marrow stromal cells. These findings indicate that the mt D4-GDI functions as a dominant negative molecule against endogenous D4-GDI.

Direct involvement of the Rho family in oncogenesis was discussed in a report [24]. Some GDS with a dbl-homology domain responsible for stimulating nucleotide exchange activity have been reported as potent oncogenes capable of transforming NIH-3T3 cells into a malignant phenotype (e.g., Dbl, Vav, and Lbc) [7,22]. Tiam1 was identified as an invasion-related gene and promoted leukemia progression through activation of the Rac signaling pathway [24]. In contrast to the function of Tiam1 in leukemic cells, Tiam1 and Rac have an invasion-suppressor role in epithelial cells [38]. Rho may also be involved in the increased mobility seen in metastasis through its control of the assembly of focal adhesions [39]. A study suggested that Rho regulates cadherin-mediated adhesion in small

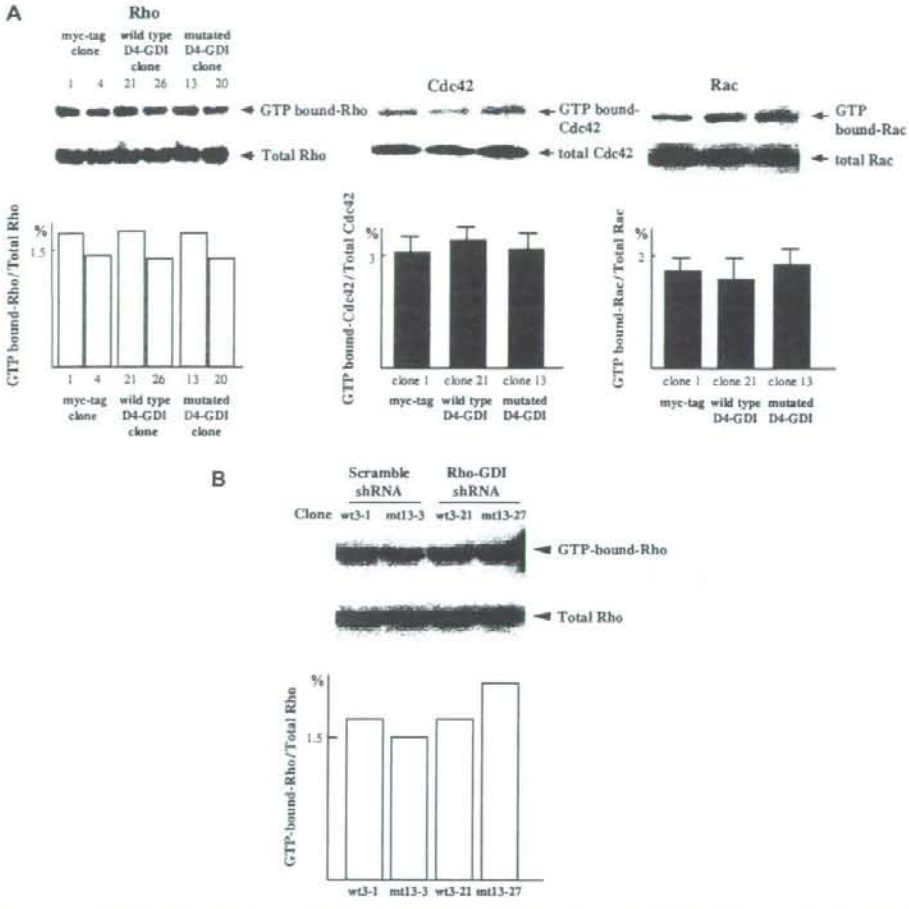

Figure 9. Detection of cellular guanine triphosphate (GTP)–bound Rho and Rac in leukemic cells. (**A**) Cells lysates were clarified by centrifugation, and equal volumes of lysates were incubated with 20 μg glutathione S-transferase (GST)–Rho-binding domain (RBD) beads. Beads were washed four times. Bound Rho proteins were detected by Western blotting using an anti-RhoA monoclonal antibody. The upper figures show the expressions of GTP-bound Rho and total Rho in all clones. The amounts of activated Rho (GTP-bound form) in all clones were almost the same. In order to quantitate the amount of GTP-bound Rho, a densitometric analysis was performed using NIH image version 1.62. The amount of RBD-bound Rho was normalized to the total amount of Rho in cell lysates for comparison of Rho activities (level of GTP-bound Rho) among different samples. The ratios of GTP-bound Rho to total Rho are shown in the lower graph. The GTP-bound Rho accounted for 1.3% to 1.6 % of total Rho in these six clones. There are no significant differences among the clones. The measurement of Rac activity was performed using the Rac Activation Assay kit (Cytoskeleton, Denver, CO, USA) according to the manufacturer's protocol. Amounts of activated Rac (GTP-bound form) in three clones were almost similar. In order to quantitate the amount of GTP-bound forms, a densitometric analysis was performed. The amount of GTP-bound Rac was normalized to the total amount of Rac in cell lysates for comparison of Rac activities among different samples. The ratios of GTP-bound Rac to total Rac are shown in the lower graph. The GTP- bound Rac accounted for 1.7% to 1.9% of total Rac in three clones, respectively. There are no significant differences among the clones. (**B**) Alterations of cellular GTP-bound Rho under the condition of decreased expression of Rho-GDI in leukemic cells with wt D4-GDI or mt D4-GDI overexpression. The pull-down assay for Rho using the wild-type or mutated D4-GDI clones (wt3-1, wt3-21, mt13-3, or mt3-27) with a vector of scramble shRNA or a vector for shRNA of Rho-GDI were done. As a result, the GTP-bound Rho in Rho-GDI knockdown mt D4 clones (mt13-27) was slightly increased compared with clones with scramble shRNA vector (wt3-1 and mt13-3) or Rho-GDI knockdown wt D4 clones (wt3-21).

cell lung carcinoma cells [40]. We reported that Rho activation augmented leukemic cell invasion through acceleration of cell adhesion, but not cell proliferation [1]. Itoh et al. [41] indicated rho-associated kinase played an essential part in tumor cell invasion, and that rho-associated kinase inhibitor may have potential as a therapy for prevention of malignant invasion and metastasis. In addition, Rho-GDI may also play a role in cancer invasion and metastasis

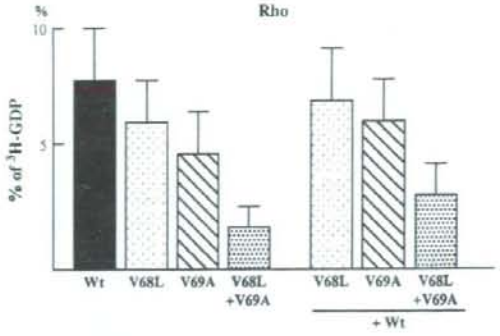

Figure 10. [³H]GDP dissociation assay of Rho. The inhibitory activities of mutated (mt) D4 with two mutations of V68L and V69A on the dissociation of [³H]GDP from isoprenylated Rho were less active than wild-type (wt) D4. The decreased dissociation activity of D4 with each single mutation (V68L orV69A) was slight. The results of the inhibitory activities of wt plus mt D4 with both mutations of V68L and V69A on the dissociation of [³H]GDP from isoprenylated Rho showed mt D4 was dominant negative of wt D4 on the dissociation of [³H]GDP from isoprenylated Rho. The dominant negative effect was not observed in the D4 with single mutation of V68L orV69A.

via involvement in the CD44 signaling pathway, because Rho-GDI coimmunoprecipitated with the CD44-ERM complex [42]. Recently, Zhang et al. reported that D4-GDI is expressed in a panel of breast cancer cell lines, but not in benign-derived mammary epithelial cells, and the D4-GDI modulates breast cancer cell–invasive activities [43]. These findings obviously indicate that the Rho family and its regulatory proteins play critical roles in the development and progression of malignancy.

Overexpression of wt D4-GDI or mt D4-GDI did not alter Rho or Rac activity, which was represented by the amount of GTP-bound Rho or Rac. D4-GDI functions both to inactivate Rho, via inhibition of the GDP dissociation from Rho, and to activate Rho, via suppression of the GTPase activity of Rho itself. Furthermore, D4-GDI has weaker GDP dissociation inhibitory activity (10-fold less) than Rho-GDI. Recently, Zhang et al. [43] reported that the activation status of Rac1, Cdc42, and RhoA was not altered as a result of D4-GDI depletion. In addition, like other Rho-GDIs, D4-GDI was postulated to bind and inhibit Rho GTPases. However, much yet remains to characterize the specificity of D4-GDI [15,16]. Although recombinant D4-GDI binds to purified Rac1, Cdc42, and RhoA, there is no evidence showing that they can form stable complexes in vivo [43]. Thus, the lack of changes in Rho or Rac activity in response to exogenous expression of wt D4-GDI or mt D4-GDI may be explained. On the other hand, the GTP-bound Rho in mt D4-GDI clone with Rho-GDI was slightly increased in contrast to mt D4-GDI clone without Rho-GDI knockdown or wt D4-GDI clones with/without Rho-GDI knockdown. These results suggest that the altered phenotypes of leukemic cells may be partially caused by Rho activation due to mt D4-GDI expression. However, the invasiveness, motility, and adhesion activity of mt D4-GDI clone with Rho-GDI knockdown was not changed in spite of the mild Rho activation in the mt D4 clone. Ishizaki et al. [44] recently report that combined disruption of both the Rho-GDI and D4-GDI genes in mice resulted in reduction of marginal zone B cells in the spleen, retention of mature T cells in the thymic medulla, and a marked increase in eosinophil numbers. Our results may be explained by the fact that the level of Rho-GDI knockdown was insufficient in contrast to the null mutation of Rho-GDI gene.

It was shown that D4-GDI is specifically cleaved at two positions (residues 18–19 and 54–55) by two different apoptosis proteases, caspase-3 and caspase-1, respectively [17,45]. These consensus cleavage sequences are not present in either Rho-GDI or Rho-GDIγ. A truncated D4-GDI cleaved by caspase-1 is unable to effectively bind and regulate Rho family members. D4-GDI is a target protein of caspase-3 in the process of anti–IgM-mediated or Fas-dependent apoptosis [17,46]. The positions of point mutations found in D4-GDI are residues 68 and 69. Therefore, the positions of these mutations are 13 and 49 amino acids from the cleavage sequence. No significant differences in the apoptosis induced by anti-cancer reagents, i.e., methotrexate, cyclohexamide, and vincristine, were seen in Raji cells transferred with mt D4-GDI transgene (data not shown).

It has been reported that Rho-GDI forms a complex with Rho A, CDC42, and Rac, while CDC42 and Rac was not found to interact with D4-GDI. Furthermore, stimulation with phorbol ester led to phosphorylation of D4-GDI in U937 cells [15]. Their results suggested that D4-GDI can regulate specific signal pathways in hematopoietic cells.

D4-GDI is a highly abundant cytoplasmic protein in lymphocytes, and has had a highly conserved primary amino acid sequence since the divergence of mammalian species. However, D4-GDI–deficient mice and in vitro embryonal stem cell differentiation analysis indicated D4-GDI expression is not essential for hematopoiesis and did not clarify its function in hematopoietic cells [47,48]. Our results indicate that D4-GDI overexpression in transformed cells changes cell motility, cell adhesion, and invasiveness in some organs. In normal lymphocytes, D4-GDI may have a subtle, yet crucial, function related to cell motility and adhesion.

Li et al. [49] reported that D4-GDI might be involved in the progression of human cutaneous T-cell lymphoma using a cDNA microarray in the clonally related T-cell lines derived from different stages of a progressive T-cell lymphoma involving skin. They found the D4-GDI gene to be one of the downregulated genes in cells from an advanced, clinically aggressive stage lymphoma, in contrast to cells from an earlier, clinically indolent stage of lymphoma. Expression of D4-GDI mRNA in cells derived from the aggressive stage lymphoma was shown to be markedly decreased as compared with cells derived from